Synthesis and evaluation of polymer-drug conjugates as potential antioxidant and cholinesterase inhibitors for neurodegenerative diseases.

MAHADIK, N., BARRON, G., KONG THOO LIN, P. and THOMPSON, C.

2024

CHEMISTRY OF MATERIALS

Open Access

pubs.acs.org/cm

Article

Synthesis and Evaluation of Polymer-Drug Conjugates as Potential Antioxidants and Cholinesterase Inhibitors for Neurodegenerative Diseases

Published as part of Chemistry of Materials special issue "Polymer-Drug Conjugate Materials."

Nuruddin Mahadik, Gemma A. Barron, Paul Kong Thoo Lin, and Colin J. Thompson*

Cite This: *Chem. Mater.* 2024, 36, 10514−10527

Read Online

ACCESS | Metrics & More | Article Recommendations | Supporting Information

ABSTRACT: Polymer-drug conjugates (PDCs) may offer improved water-solubility and *in vitro* activity of potential antioxidant and cholinesterase (ChE) inhibitor drugs compared to the drugs alone. Conjugation of these potential drugs to water-soluble polymers could increase their therapeutic efficacy. Vanillin was conjugated to poly(allylamine hydrochloride) (NM10 and NM15) and naphthalimidohexylamine (HEXNAP) was conjugated to poly(acrylic acid) (N5 and N10). The antioxidant and cholinesterase inhibitory activities of these novel PDCs were evaluated and compared with those of their respective starting materials. Additionally, *in silico* molecular modeling studies were conducted to explore the potential cholinesterase inhibitory mechanisms of these conjugates. NM15 (unadjusted and adjusted value) showed significantly enhanced *in vitro* antioxidant activity ($p \leq 0.0001$) compared to vanillin. The adjusted value of N5 compared to HEXNAP showed significantly enhanced *in vitro* cholinesterase inhibitory activity against acetylcholinesterase (AChE) and butyrylcholinesterase (BuChE) ($p \leq 0.0001$). Kinetic and molecular modeling studies revealed that N5 was a competitive inhibitor of butyrylcholinesterase and interacted with the active sites of human acetylcholinesterase and human butyrylcholinesterase enzymes. NM15 and N5 were identified as lead PDCs based on their enhanced antioxidant and cholinesterase inhibitory activity, respectively. Overall, this work demonstrates the potential use of PDCs as treatment options for neurodegenerative diseases.

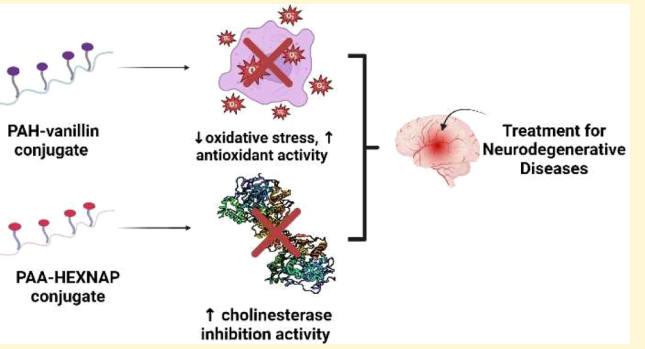

1. INTRODUCTION

Neurodegenerative diseases (NDs), such as Alzheimer's disease (AD), Parkinson's disease, Huntington's disease, and amyotrophic lateral sclerosis, are marked by the progressive degeneration of neurons and the accumulation of protein aggregates.[1,2] These conditions result in the gradual loss of neuronal cells and a decline in their functionality, leading to cognitive and behavioral impairments.[2] According to the World Health Organization (WHO), neurological disorders are projected to become the second leading cause of death globally within the next 20 years.[2] The complex etiology of these diseases, involving numerous endogenous factors, genetic influences, and environmental conditions, currently limits treatment options to symptomatic management.[3,4] While these treatments can improve cognitive performance, they do not delay or reverse the progression of these diseases.[4,5]

Oxidative stress (OS) is a common feature of neurodegenerative diseases (NDs) and may significantly contribute to the dysfunction or death of neuronal cells, thereby playing a key role in the disease's pathogenesis.[1] Additionally, decreased cholinergic activity in the central nervous system (CNS) is a crucial factor in the cognitive deficits associated with NDs.[6,7] Acetylcholinesterase (AChE) influences the pathogenesis of these diseases through its effects on the inflammatory response, apoptosis, OS, and the aggregation of pathological proteins.[6]

Alzheimer's disease (AD), the most prevalent type of dementia, is a progressive, neurodegenerative disease. In contemporary AD therapy, symptomatic treatment is the only option due to its complex etiology.[3] Current pharmacological treatments that are now being developed or evaluated in clinical trials target the primary pathological hallmarks of AD: amyloid β (Aβ) plaques and neurofibrillary tangles (NFTs).[8] These pathological hallmarks are driven by oxidative stress (OS) and cholinesterase activity.[9] OS, an early AD trigger, contributes to Aβ plaque formation and tau aggregation in NFTs.[10,11] Current

Received: June 25, 2024
Revised: October 16, 2024
Accepted: October 16, 2024
Published: October 23, 2024

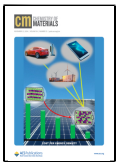

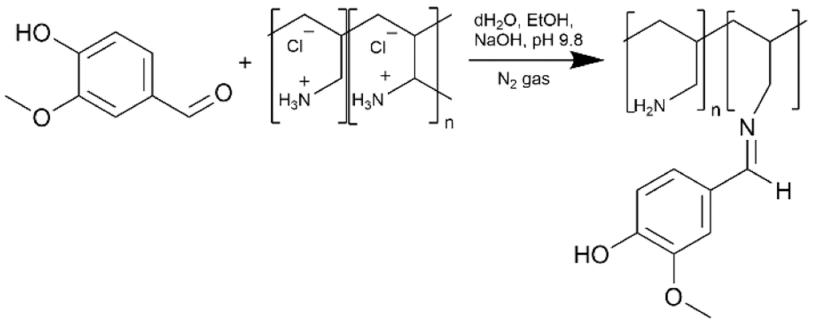

Figure 1. Illustration of PAH and Vanillin conjugate synthesis.

observations indicate that as the AD progresses, butyrylcholinesterase (BuChE) activity increases and AChE activity decreases, linking increased cholinesterase activity to tau tangle formation.[12,13]

Significant progress has been made in the synthesis of small multitargeted molecules acting as both antioxidants and cholinesterase inhibitors.[9,14−17] In recent years, the use of antioxidants, e.g., vanillin and its derivatives, has been reported for treating AD.[9,18−20] Naphthalimide derivatives have been extensively studied due to their broad range of action against pharmacologically significant targets.[21,22] For AD specifically, vanillin and naphthalimide derivatives encompass the ability to counteract OS, reduce inflammation, and inhibit cholinesterase (ChE) activity.[9,23] However, vanillin and naphthalimide exhibit low water-solubility and limited uptake resulting in low bioavailability.[24,25]

Polymer-drug conjugates (PDCs) are promising candidates for treating NDs. These therapeutic compounds involve the covalent attachment of drugs to water-soluble polymers, which offers several advantages: enhanced solubility, improved bioavailability, and increased stability. PDCs can also reduce toxicity, extend circulation time, and incorporate targeting moieties and imaging agents for precise targeting. Additionally, they enable controlled drug release through cleavable linkers in specific environments.[26] Moreover, PDCs exhibit greater chemical stability in plasma, reduced immunogenicity, and smaller particle sizes (<50 nm), facilitating enhanced penetration compared to alternative nanocarriers like micelles and liposomes.[26] There are currently only a few studies on PDCs for the treatment of neurological conditions.[27−31] These studies, however, demonstrated that the PDCs were stable in a physiological environment, nontoxic, and showed targeted uptake and drug transport to the brain, making them a potential treatment strategy for NDs.

Therefore, this research was focused on the development of novel polymer-vanillin and polymer-naphthalimidohexylamine conjugates for NDs treatment. Poly(allylamine hydrochloride) (PAH), a synthetic cationic, pH-sensitive polymer was chosen for conjugation with vanillin as it provides water-solubility, biocompatibility, and has been shown to form polyplexes with good stability.[32−34] Polyacrylic acid (PAA), a synthetic polyanionic, nontoxic, biocompatible, and biodegradable polymer, was chosen for conjugation with naphthalimidohexylamine (HEXNAP). Due to their stability and biocompatibility, nanoparticles derived from PAA derivatives can be employed to deliver drugs,[35] and attaching these active moieties to water-soluble polymers will increase their aqueous solubility.[26,36]

The objectives were to (i) synthesize and characterize a series of novel PAH-vanillin and PAA-HEXNAP conjugates, (ii) evaluate their *in vitro* antioxidant and cholinesterase inhibitory activities, and (iii) explore their potential cholinesterase inhibitory mechanism through *in silico* molecular modeling studies. This comprehensive approach not only aims to provide novel therapeutic avenues for NDs but also paves the way for future research and development in PDCs for neurological applications.

2. MATERIALS AND METHODS

2.1. Materials. Poly(allylamine hydrochloride) (M_W = 17,500 g/mol), vanillin, 1,6-diaminohexane, naphthalic anhydride, (1-ethyl-3-(3-(dimethylamino)propyl)carbodiimide hydrochloride) (EDC), ethanol, 2,4,6-tri(2-pyridyl)-*s*-triazine (TPTZ), ferric chloride, trolox, gallic acid, galantamine, folin, and ciocalteu's phenol reagent, sodium carbonate, sodium acetate, sodium hydroxide, glacial acetic acid, *Electrophorus electricus*, equine serum (5,5′-dithiobis(2-nitrobenzoic acid) (DTNB)), sodium phosphate, Hepes, acetylthiocholine iodide (AChEI), and butyrylthiocholine iodide (BuChEI) were purchased from Sigma-Aldrich (Dorset, U.K.). Polyacrylic acid (M_W = 25,000 g/mol) was purchased from Fujifilm Wako Pure Chemical Corporation (Osaka, Japan). 2,2-diphenyl-1-picrylhydrazyl (DPPH) and tacrine were purchased from TCI, (Tokyo Chemical Industry, U.K.). The solvents for the ^{1}H Nuclear Magnetic Resonance (NMR) analysis of D_2O and $CDCl_3$ were obtained from Cambridge Isotope Laboratories, Inc.

2.2. Methods. *2.2.1. Synthesis of PAH-Vanillin Conjugates.* PAH-vanillin conjugates were synthesized as described by Wang et al.,[37] with some adjustments. Vanillin was conjugated to a fixed amount of PAH using a condensation reaction employing different molar ratios (Figure 1).

A solution of PAH (0.2336 g; 2.5 mmol in the means of the monomer) in H_2O (30 mL) was adjusted with NaOH to pH 9.8. The solution of vanillin (0.25 mmol (10%) and 0.375 mmol (15%)) in ethanol (10 mL) was slowly added under stirring to the PAH solution while the PAH solution was purged with nitrogen gas. The solution was agitated overnight at ambient temperature followed by dialysis (with a molecular weight cutoff of 3500 Da) with water (5 L) for 24 h, with 6 water changes occurring during that time frame. The dialyzed products were next subjected to freeze-drying using the VirTis advantage freeze-dryer (Biopharma Process System, U.K.). The products NM10 (10% vanillin attached, yield 65.1 ± 2.2%) and NM15 (15% vanillin attached, yield 68.6 ± 0.6%) were obtained. The confirmation of structural changes was conducted using ^{1}H NMR, ATR-FT-IR, and UV−visible spectroscopy. Elemental analysis was done on NM15 only.

NM10 ^{1}H NMR: (D_2O solvent peak $\delta_{4.70}$), $\delta_{9.31}$ (HC = N, imine), $\delta_{6.56}$, $\delta_{7.18}$ (3H, Ar-H, Vanillin), $\delta_{3.74}$ (−OCH_3, Vanillin), $\delta_{1.64}$ (CH, branch chain of PAH), $\delta_{1.22}$, and $\delta_{2.70}$ (CH_2, branch chain of PAH). NM15 ^{1}H NMR: (D_2O solvent peak $\delta_{4.45}$), $\delta_{9.01}$ (HC = N, imine), $\delta_{6.31}$, $\delta_{6.77}$ (3H, Ar-H, Vanillin), $\delta_{3.408}$ (−OCH_3, Vanillin), $\delta_{1.32}$ (CH, branch chain of PAH), $\delta_{0.88}$, $\delta_{2.41}$ (CH_2, branch chain of PAH).

2.2.2. Synthesis of Naphthalimidohexylamine. The synthesis of HEXNAP (Figure 2) was conducted following the methodology previously described by Blaikie et al.,[9] with some adjustments. A solution of 1,6-diaminohexane (2.35 g, 20.20 mmol) and naphthalic

https://doi.org/10.1021/acs.chemmater.4c01767
Chem. Mater. 2024, 36, 10514−10527

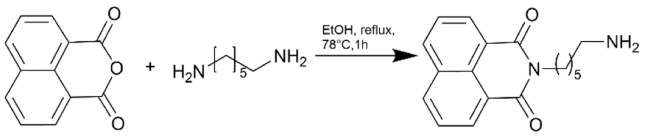

Figure 2. Illustration of naphthalimidohexylamine synthesis.

anhydride (2.00 g, 10.10 mmol) in ethanol (100 mL) was heated under reflux at approximately 78 °C for 1h. The solution was allowed to cool to ambient temperature, and the solid byproduct (bisnaphthalimide) formed was separated by filtration using a Buchner funnel. The ethanol filtrate was dried by evaporation by using a Büchi R-210 rotary film evaporator (BUCHI, U.K.). The residue was subjected to water treatment, resulting in the formation of a precipitate that was filtered off with water and dried in a vacuum oven (yield 51.9%). Thin-layer chromatography (TLC) was employed to verify the purity of the sample, while ^{1}H NMR spectroscopy was utilized for comprehensive characterization.

^{1}H NMR: ($CDCl_3$ solvent peak $\delta_{7.29}$): $\delta_{8.6}$ (dd, 2H, napth-H), $\delta_{8.2}$ (dd, 2H, napth-H), $\delta_{7.8}$ (t, 2H, napth-H), $\delta_{4.2}$ (t, 2H, N−CH2-CH2), $\delta_{2.8}$ (t, 2H, CH2-CH2-NH2), $\delta_{1.8-1.75}$ (m, 4H, CH2-CH2-CH2), $\delta_{1.5-1.44}$ (m, 4H, CH2-CH2-CH2).

2.2.3. Synthesis of PAA-HEXNAP Conjugates (Figure 3). A solution of PAA (0.2305 g; 3.2 mmol in the means of monomer) and EDC (1.2 equiv of HEXNAP) in methanol (30 mL) was refluxed at 50°C and stirred for 2 h. A solution of HEXNAP (0.16 mmol (5%) and 0.32 mmol (10%)) in DMSO (20 mL) was slowly added while stirring of the PAA-EDC solution which was purged with nitrogen gas. The solution was left stirring overnight at ambient temperature followed by dialysis (with a molecular weight cutoff of 3500 Da) with water (5 L) for 24 h, with 3 water changes occurring during that time frame. The dialyzed product was filtered and transferred to the round-bottom flask (RBF) and 1 M $NaHCO_3$ (15 mL) was added, and the solution was agitated overnight at ambient temperature followed by dialysis (with a molecular weight cutoff of 3500 Da) with water (5 L) for 24 h, with 6 water changes. The dialyzed product was filtered and freeze-dried using the VirTis advantage freeze-dryer. The products N5 (5% HEXNAP attached, yield 60.8 ± 5.4%) and N10 (10% HEXNAP attached, yield 57.3 ± 18.4%) were obtained. The confirmation of structural changes was conducted using ^{1}H NMR, ATR-FT-IR, and UV−visible spectroscopy. Elemental analysis was done on N5 only.

N5 ^{1}H NMR: (D_2O solvent peak $\delta_{4.75}$), $\delta_{8.1}$ (dd, 2H, napth-H), $\delta_{8.0}$ (dd, 2H, napth-H), $\delta_{7.5}$ (t, 2H, napth-H), $\delta_{2.1}$ (C<u>H</u>, aliphatic chain of PAA), $\delta_{1.43}$ (C<u>H$_2$</u>, aliphatic chain of PAA). N10 ^{1}H NMR: (D_2O solvent peak $\delta_{4.75}$), $\delta_{8.1}$ (dd, 2H, napth-H), $\delta_{7.8}$ (dd, 2H, napth-H), $\delta_{7.25}$ (t, 2H, napth-H), $\delta_{2.1}$ (C<u>H</u>, aliphatic chain of PAA), $\delta_{1.44}$ (C<u>H$_2$</u>, aliphatic chain of PAA).

2.2.4. Structural Characterization Using Nuclear Magnetic Resonance (NMR). ^{1}H NMR characterization was performed using a BRUKER Ascend 400 MHz Avance III HD instrument (Bruker, Coventry, U.K.) with Mnova NMR software (Mestrelab Research) with scans ranging from 16 to 128. D_2O was used as a solvent for each product except for HEXNAP where $CDCl_3$ was used. The % of drug conjugation to the polymer was calculated using NMR.

2.2.5. Elemental Analysis. Polymer-drug conjugation of NM15 and N5 was also calculated by using elemental analysis. To constrain the total concentrations of C, N, and H in the samples, ca. 1.5−2 mg was weighed (tin capsule, 8 mm height, 5 mm diameter from Elemental Microanalysis) and analyzed by flash-combustion with an elemental analyzer (EA, Isolink from Thermo Fisher Scientific). The EA was equipped with a zero-blank autosampler and a combustion column packed with CuO and Cu wire held at 950 °C. Helium was used as a carrier gas at a constant flow rate of 140 mL/min. The He reference flow was set to 100 mL/min. For the combustion, a pulse of O_2 gas was injected for 5 s at a flow rate of 250 mL/min. The gas chromatograph oven in the EA was held at 65 °C. Measurements with a thermal conductivity detector were calibrated against a series of acetanilide standards. All samples were run in duplicates, and a blank was inserted after each sample was analyzed.

2.2.6. Structural Characterization Using Fourier Transform Infrared Spectroscopy (FT-IR-ATR). FT-IR analysis was performed using a Nicolet is10 instrument with an ATR attachment (Thermo Scientific, U.K.) and using OMNIC software. The background was collected first, and then the sample with a total of 16 scans. The scan range was between 4000 and 500 cm^{-1}.

2.2.7. Structural Characterization Using UV−Visible Spectroscopic Analysis. The UV−visible spectra of all compounds were determined using a Cary 60 UV−visible spectrophotometer (Agilent, U.K.). Compounds were dissolved in dH_2O and further diluted to get an absorbance value below 1. Solutions were scanned from 190 to 500 nm in a quartz cell. Spectra were recorded by using Carry WinUV software.

2.2.8. Total Phenolic Content: The Folin-Ciocalteu (FC) Assay. The FC assay was carried out as previously reported by Pohl et al.,[38] with minor modifications. Gallic acid (1 mg/mL, ethanol: water (4:10)) stock solution was diluted to a concentration range between 0.006 and 0.20 mg/mL. All compounds (NM10, NM15, N5, N10, vanillin, HEXNAP, PAA, PAH, and trolox (positive control)) were prepared in an ethanol: water (4:10) mixture. A dilution series of all compounds ranging from 0.003 to 2 mg/mL was made in Eppendorf tubes (1.5 mL). For the reaction to occur, 25 μL of compounds and negative control (ethanol: water (4:10)) were added to a 96-well plate in triplicates. dH_2O (200 μL) and FC reagent (20 μL) were added to all of the wells and incubated for 3 min in the dark. After incubation, 20% Na_2CO_3 (25 μL) was added to all of the wells, and the plate was incubated for 30 min at 37 °C in the dark. After incubation, absorbance was read at 750 nm using a Bio-Rad iMark UV−vis microplate reader (Bio-Rad, U.K.). The results are expressed as mg gallic acid equivalents (GAE) per gram dry sample (C).

2.2.9. In Vitro Antioxidant Activity. 2.2.9.1. 2,2-Diphenyl-1-picrylhydrazyl (DPPH) Assay. The DPPH assay was carried out as previously reported by Scipioni et al.,[18] with minor modifications. All compounds (NM10, NM15, N5, N10, vanillin, HEXNAP, PAA, PAH, and gallic acid (positive control)) were prepared in an ethanol: water (4:10) mixture. A dilution series of all compounds ranging from 0.1 to 10,000 μg/mL was made in Eppendorf tubes (1.5 mL). For the reaction to occur, 50 μL of compounds and negative control (ethanol: water (4:10)) were added to a 96-well plate in triplicates. DPPH solution (100 μL, 0.1 mM) was added to all of the wells. Plates were analyzed every 15 min for up to 120 min and absorbance was read at 517 nm using a Bio-Rad iMark UV−vis microplate reader. Results were expressed in terms of IC_{50} (concentration at which 50% of the radical scavenging activity was achieved).

2.2.9.2. Ferric-Reducing Antioxidant Power (FRAP) Assay. The FRAP assay was carried out as previously reported by Pohl et al.,[38] with minor modifications. A stock solution of Trolox (1 mg/mL) was prepared in an ethanol: water (4:10) mixture and further diluted to 0.002−0.08 mg/mL with dH_2O. All compounds (NM10, NM15, N5, N10, vanillin, HEXNAP, PAA, PAH, and gallic acid (positive control)) were prepared in the ethanol: water (4:10) mixture. A dilution series of all compounds ranging from 0.002 to 2 mg/mL was made in Eppendorf tubes (1.5 mL). For the reaction to occur, 10 μL of compounds and the negative control (ethanol: water (4:10)) were added to a 96-well plate in triplicate. FRAP reagent (190 μL) was added to all wells and incubated for 30 min at 37 °C in the dark. After incubation, the absorbance was read at 593 nm using a Bio-Rad iMark 18 UV−vis microplate reader. The results are expressed as milligrams of Trolox equivalent (TE) per gram of dry sample (C).

2.2.10. In Vitro Cholinesterase Inhibitory Activity. 2.2.10.1. Ellman's Assay. The inhibitory activity of the PDCs against AChE and BuChE was determined using an Ellman's assay as previously reported by Blaikie et al.,[9] with minor modifications. AChE and BuChE stock solutions (22 U/mL) from *E. electricus* and equine serum, respectively, were prepared in 20 mM Tris HCl (pH 7.5). Before use, AChE and BuChE stock solutions were diluted 1:100 and 3:100, respectively. A 3 mM DTNB (5,5′-dithiobis(2-nitrobenzoic acid)) solution was prepared in phosphate/Hepes buffer (0.05 M/0.09 M, pH 7.5). Solutions of 15 mM acetylthiocholine iodide (AChEI) and butyrylthiocholine iodide (BuChEI) were prepared in dH_2O. All

https://doi.org/10.1021/acs.chemmater.4c01767
Chem. Mater. 2024, 36, 10514−10527

Table 1. FT-IR Results for Vanillin, PAH, and NM15

	wavenumbers (cm^{-1})							
	aldehyde		hydroxyl	methoxy		amine	alkyl	imine
compounds	C = O	C−H	O−H	$O-CH_3$	CH_3	−N−H	C−H	C = N
vanillin	1660	2858	1263	1024	2944			
			3134					
PAH						1557	2914	
						3345		
NM15			1283	1025		3346	2911	1630

compounds (NM10, NM15, N5, N10, vanillin, HEXNAP, PAA, PAH, and positive controls (galantamine and tacrine)) were prepared in 10 mM Tris:HCl buffer, pH 7.4. A dilution series of all compounds ranging from 8−2000 μg/mL for AChE and 0.008−2000 μg/mL for BuChE were made in Eppendorf tubes (1.5 mL). For the reaction to occur, 125 μL of DTNB solution, 25 μL of samples and negative control (Tris:HCl buffer, pH 7.4), and 25 μL of diluted AChE or BuChE solution were added to a 96-well plate in triplicate. The plate was incubated for 10 min at 37 °C, 25 μL of AChEI and BuChEI solution were added to all wells, and the plate was incubated for a further 20 min. The absorbance was measured at 415 nm by using a BioTek Synergy HT microplate reader (Agilent, U.K.). The cholinesterase inhibitory activity was expressed in terms of IC_{50} (concentration at which 50% of the cholinesterase activity was inhibited).

2.2.10.2. Kinetic Study of BuChE Inhibition. For the kinetic study, N5, HEXNAP, and tacrine were tested at $IC_{50}/2$, IC_{50}, and $2*IC_{50}$ (these concentrations were selected from Ellman's assay results). Four concentrations of the BuChEI substrate were prepared, ranging from 5 to 50 mM. N5, HEXNAP, and tacrine were evaluated against each concentration of the substrate. The method was as described in Section 2.2.10.1 until the substrate was added to the plate in triplicate, at which point the absorbance was measured every min for 20 min at 415 nm using a BioTek Synergy HT microplate reader. For each substrate concentration, the absorbance was plotted against time, and the slope was taken as the rate (v). The reciprocal of substrate concentration ($1/S$) and rate ($1/v$) were plotted for each compound concentration and the negative control. This generated the Lineweaver−Burke plot, which could be used to determine the V_{max} and K_m values for each compound concentration and negative control.

2.2.10.3. Molecular Modeling. PyRx 0.8 was used to determine *in silico* predictions of the binding potential of N5, HEXNAP, galantamine, and tacrine with ChE enzymes. Protein structures used in the docking processes were obtained from the Protein Data Bank (human AChE - 4PQE; human BuChE - 2J4C). Both structures exhibited a resolution of less than 3 Å. Water molecules and any ligands linked to the structures were removed, while polar hydrogens were introduced. The three-dimensional (3D) structures of N5, HEXNAP, and galantamine were obtained with ChemDraw (ChemDraw Professional 22.0 and Chem3D 22.0) and the MM2 energy minimization program, and they were stored as pdb files. Each ligand and macromolecule were applied to PyRx, and the binding energies of the various conformations were calculated using Autodock Vina 1.1.25. The molecules were docked by placing a grid box around the binding sites. The binding site's position was established by employing a residue crucial to ligand binding (human AuChE- Trp86 and human BuChE- Trp82) in the enzyme active site. The grid box size was chosen to 40 Å × 40 Å × 40 Å. The lowest energy conformation for each ligand-macromolecule complex was chosen for further investigation, and the complex was loaded into BIOVIA Discovery Studio, version 21.1.0.20298 (Dassault Systèmes) for visualization.

2.3. Statistical Analysis. All experiments were conducted at least three times unless otherwise stated and results are shown as mean ± SD/SEM. Statistical analysis was performed using both Microsoft Excel 2019 and GraphPad Prism 10 (GraphPad Software), and a significant difference was determined using the one-way ANOVA and Dunnett's multiple comparisons tests (*$p < 0.05$, **$p < 0.01$, ***$p < 0.001$ ****$p < 0.0001$, ns not significant compared to solvent control).

3. RESULTS AND DISCUSSION

3.1. Synthesis and Characterization of PAH-Vanillin and PAA-HEXNAP Conjugates. In recent years, numerous polymer conjugates of various polyphenols and other small molecular drugs have been reported, demonstrating enhanced characteristics such as improved water-solubility, biocompatibility, and reduced toxicity.[31,39,40] However, to the best of our knowledge, derivatives of PAH conjugated to vanillin and PAA conjugated to HEXNAP have not been previously reported. Therefore, one of this study's objectives was to synthesize and characterize, for the first time, PAH-vanillin and PAA-HEXNAP conjugates as a potential treatment strategy for treatment of NDs.

PAH-vanillin conjugates were prepared by the reaction between the aldehyde group of vanillin and the primary amine groups of PAHs using a condensation reaction (Figure 1). In the NM15 ^{1}H NMR spectra, the peak of aromatic proton and methoxy proton of vanillin was identified around $\delta_{6.31}$, $\delta_{6.77}$ (3H, Ar−H), and $\delta_{3.408}$ ($-OCH_3$) (Figure S1). The peak for the imino (HC = N) proton was identified at $\delta_{9.31}$ (similar proton peaks were identified on NM10 spectra (Figure S2)) which was absent in PAH (Figure S4) and the parent compound vanillin which has a peak for the aldehyde (HC = O) proton around $\delta_{9.49}$ (Figure S3). According to Marin et al.,[40] the imino proton peak can also shift to a higher field due to the lower conjugation of imino linkage induced by the aliphatic nature of the polymer. It is sometimes difficult to determine the presence of imine proton peak just by NMR characterization alone when the polymer is involved in the synthesis, unlike small molecule drugs. However, these conjugates are novel compounds with no equivalent data in the literature; therefore, to prove that the conjugation was successful, further characterization was done using ATR-FT-IR and UV−visible spectroscopy.

In the ATR-FT-IR spectrum, vanillin showed a vibrational band at 1660 and 2858 cm^{-1} corresponding to the stretching of the C = O and C−H bonds in the aldehyde group, whereas the band at 1263 and 3134 cm^{-1} was due to the bending and stretching of the O−H in the hydroxyl group. The bands at 1024 and 2944 cm^{-1} were recognized as $O-CH_3$ and CH_3 stretching vibrations associated with the vanillin methoxy group.[41] PAH showed a vibration band at 1557 and 3345 cm^{-1} corresponding to N−H bending and stretching. The broad band at 2914 cm^{-1} corresponds to C−H vibrations in the PAH structure. Evidence for imine-bond formation was supported by the appearance of the vibration band at 1630−1632 cm^{-1} for C═N in the FTIR spectra,[40,42] in NM10 and NM15. The intensity at 1557 and 3345 cm^{-1} bands of amine bond present in PAH decreased and the band at 1660 cm^{-1} related to the aldehyde group present in vanillin completely disappeared. Additional bands associated with vanillin and PAH are also observed in the conjugates (Table 1 and Figures S5−S8).

https://doi.org/10.1021/acs.chemmater.4c01767
Chem. Mater. 2024, 36, 10514−10527

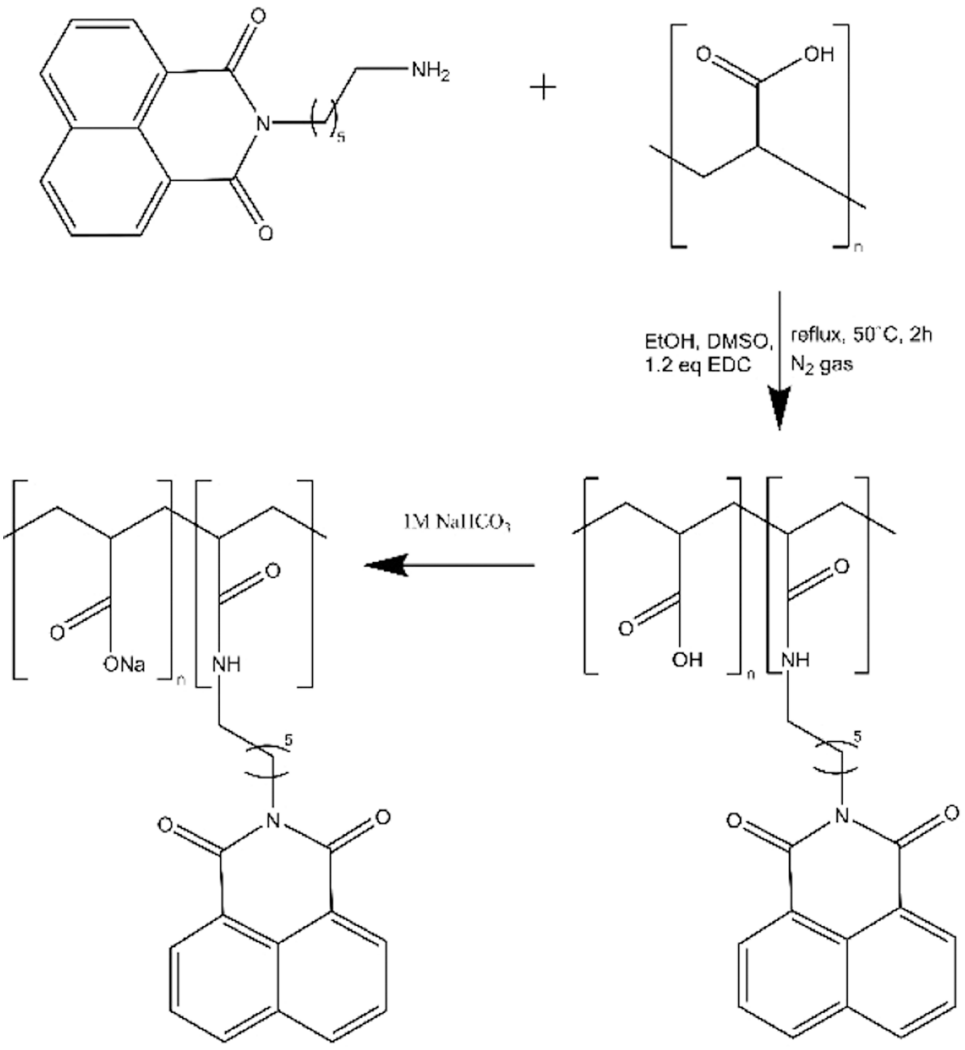

Figure 3. Illustration of the conjugate. Synthesis of PAA and naphthalimidohexylamine.

The UV−visible spectra of NM15 (representative of NM10, Figure S9) compared to vanillin and PAH are depicted in Figure 4A. Pure vanillin showed four peaks, 205, 230, 280, and 310 nm, which correspond to previously published values.[43] PAH showed no absorbance peaks, as it does not have a chromophore in its structure. One new peak appeared at around 385−390 nm for NM10 and NM15 which belong to the Schiff base bond, resulting in the generation of a new transition n-π^*.[42] In further work, the pH of the NM15 solution was adjusted to an acidic pH of 1−2 from its initial value of pH 6.7 to observe any potential impact on the UV−visible spectra. It was evident from Figure 4B that the imino bond peak at 390 nm underwent hydrolysis as the peak at 390 nm disappeared and the peak for vanillin was produced back. The pH value was critical for controlling the equilibrium of the reaction. Highly acidic pH can have a substantial impact on the formation and breakage of imino bonds. The latter are stable in alkaline or neutral conditions but hydrolyze in acidic environments.[44]

The ATR-FT-IR and UV−visible spectra data correlate with the NMR data, indicating that the vanillin moiety was successfully conjugated to the PAH polymer.

Naphthalimide derivatives have demonstrated promising therapeutic potential for AD, exhibiting antioxidant, anticholinesterase, and amyloid aggregation inhibitory activities.[9,23] Among these, the HEXNAP-vanillin conjugate has shown notable antioxidant and anticholinesterase properties.[9] However, HEXNAP is primarily soluble in organic solvents, thus limiting its use. Therefore, novel water-soluble PAA-HEXNAP conjugates were developed to enhance water-solubility and improve efficacy.

PAA-HEXNAP conjugates were prepared by the reaction between the primary amine group of HEXNAP and the carboxylic acid groups of PAA using EDC-mediated amide-bond formation (Figure 3). In the ^{1}H NMR spectra of N5, the peaks of the aromatic protons of the HEXNAP groups, which were absent in PAA, appeared at $\delta_{8.1}$ (2H, napth-H), $\delta_{8.0}$ (2H, napth-H), and $\delta_{7.5}$ (2H, napth-H) (Figures S10, S12, and S13). Similar peaks were seen for the N10 conjugate (Figure S11). In the ATR-FT-IR spectrum, HEXNAP showed stretching bands at 3306 cm^{-1} corresponding to primary amine, 1654 and 1695 cm^{-1} assigned as the ring C = O, and 2930 and 2854 cm^{-1} corresponding to the hexyl chain. PAA showed vibration bands at 1694, 1159, and 1149 cm^{-1} corresponding to C = O, −(C−O)H, and COO$^-$ stretching and bending of carboxylic acid. The bands at 2931 and 1410 cm^{-1} correspond to the stretching and bending of C−H and C−H$_2$ vibrations in the PAA structure.[45] Evidence for amide-bond formation was supported by the appearance of the vibration band at 3252−3196 cm^{-1} for N−H

https://doi.org/10.1021/acs.chemmater.4c01767
Chem. Mater. 2024, 36, 10514−10527

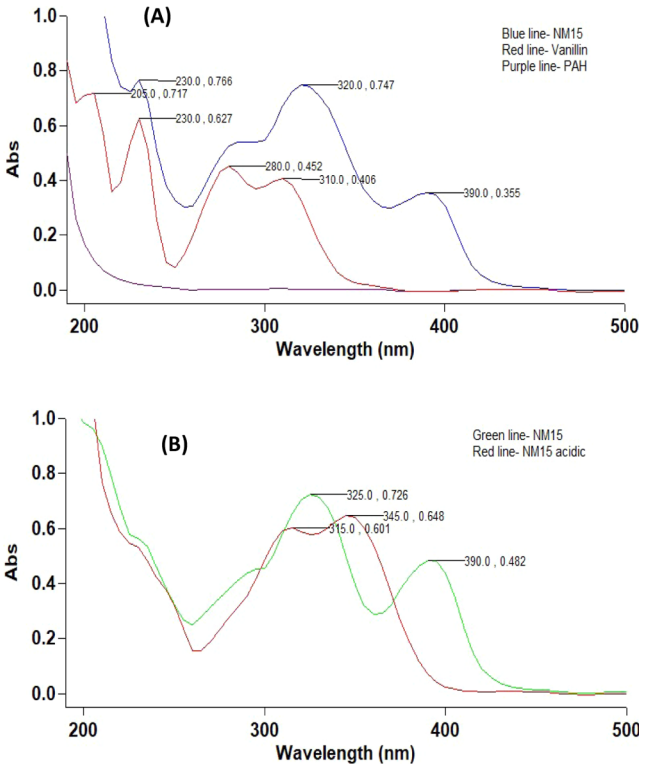

Figure 4. UV−visible spectroscopic analysis of (A) NM15 and (B) NM15 at acidic pH.

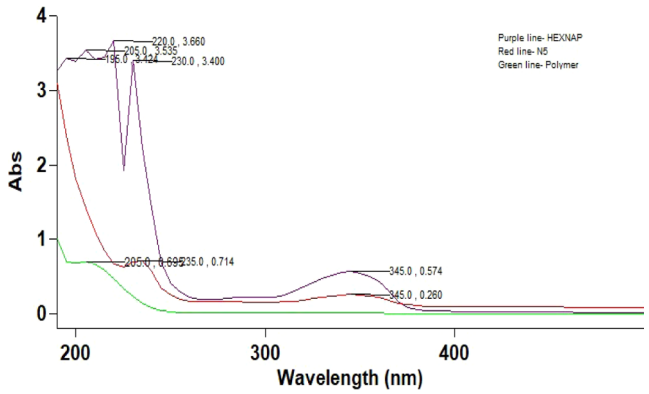

Figure 5. UV−visible spectroscopic analysis of N5.

and 1557−1552 cm^{-1} for C = O in the FTIR spectra,[31,46] of N5 and N10. Additional bands associated with vanillin and PAH are also observed in the conjugates (Table 2 and Figures S14−S17).

Similarly, the UV−visible spectra of N5 (representative of N10, Figure S18) compared to HEXNAP and PAA are depicted in Figure 5. N5, N10, and HEXNAP had a peak at 345 nm which corresponds to the 1,8 naphthalic ring of HEXNAP.[47] These data confirm that the HEXNAP moiety was successfully conjugated to the PAA polymer.

Furthermore, integration values of the NMR spectroscopy can be employed to determine the % conjugation of the drug to the polymer.[48] An example calculation for NM15 is shown below where 3 is the PAH proton integration value and 0.41 is the combined integration value of the hydrogen atoms in the vanillin aromatic ring (Figure S1). Each integration value was then divided by the total number of protons, and the resulting value was used to determine % conjugation.

$$\frac{3}{3} = 1$$

$$\frac{0.41}{3} = 0.136$$

$$\left(\frac{0.136}{1}\right) \times 100 = 13.6\%$$

Conjugation percentages were determined for each PDC, and results are presented in Table 3. NM10 and NM15% attachments were closest to the theoretical value; however, this was not the case for N5 and N10. This could be due to the hydrophobic nature of HEXNAP which may have hindered its interaction with the polymer. Due to the limitations of NMR, such as overlapping peaks and a noisy baseline, it was difficult to determine the exact percentage of the drug attached to the polymer. Therefore, the % conjugation achieved was also calculated using elemental analysis for NM15 and N5 (Table 3). For example, the analysis of NM15 revealed a composition of 53.01% carbon, 8.14% hydrogen, and 14.22% nitrogen. These data indicated an excess of 1.418 mol of carbon, attributable to the vanillin. By correlating this excess carbon with vanillin, the percentage of vanillin attached was determined to be 17.7%. Data obtained from elemental analysis provide a more reliable method for determining the percent conjugation of lead compounds than NMR, which is limited by overlapping peaks and a noisy baseline. Therefore, all further calculations are based on elemental analysis data.

To further elucidate the benefits of these novel conjugates, their total phenolic content, antioxidant properties, and cholinesterase inhibitory activity were thoroughly investigated.

Table 3. % Conjugation of PDCs Derived from ^{1}H NMR and Elemental Analysis Data (n = 3, Mean ±SD)

theoretical % conjugation	calculated % conjugation by ^{1}H NMR	calculated % conjugation by elemental analysis
NM10-10%	9.3 ± 0.9	NA
NM15-15%	14.6 ± 1.4	17.9 ± 0.3
N5-5%	0.24 ± 0.08	1.04 ± 0.03
N10-10%	1.1 ± 0.1	NA

Table 2. FT-IR Results for HEXNAP, PAA, and N5

	wavenumbers (cm^{-1})								
	amine	HEXNAP ring	carboxylic acid			amide		alkyl chain	
compounds	−N−H	C = O	C = O	−(C−O)H	$-COO^-$	N−H	C = O	C−H	$C-H_2$
HEXNAP	3306	1695, 1654						2930, 2854	
PAA			1694	1159	1449			2931	1410
N5		1658	1698		1450	3196	1552	2930, 2854	1402

https://doi.org/10.1021/acs.chemmater.4c01767
Chem. Mater. 2024, 36, 10514−10527

3.2. Determination of Total Phenolic Content. The total phenolic content of the PDCs and starting materials was determined using the Folin-Ciocalteu (FC) assay (Figure 6).

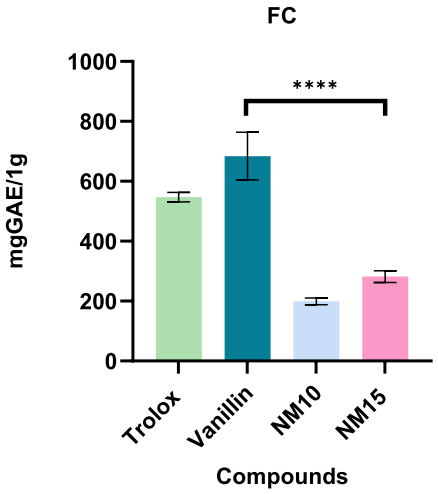

Figure 6. Total phenolic contents of NM10 and NM15. Data presented as mean ± SD (n = 3), significant difference *via* one-way ANOVA (****$p \leq 0.0001$), and Dunnett's multiple comparisons tests.

Phenolic compounds possess hydroxyl groups that play a significant role in their ability to scavenge free radicals.[49] The highest total phenolic content was found for NM15 (282 ± 20 mgGAE/1 g). As per elemental analysis % attachment data (Section 3.1), only 17.8% of vanillin was attached in NM15 conjugate; thus, the adjusted NM15 exhibited a higher proportional phenolic content compared to vanillin (684 ± 80 mgGAE/1 g). For example, the 17.9% (NM15) total phenolic content of vanillin is 122.4 mgGAE/1 g much lower than NM15. The enhanced conjugation activity can be attributed to the formation of an imino bond, resulting in the formation of phenolic Schiff bases.[50] These Schiff bases are widely recognized for their potent antioxidant properties and ability to effectively scavenge free radicals through the mechanism of hydrogen atom transfer (HAT) or single electron transfer (SET).[50] Due to the absence of phenolic groups, PAH, PAA, HEXNAP, N5, and N10 did not exhibit any phenolic content (results not shown). These findings indicate that NM10 and NM15 may have antioxidant properties.

3.3. *In Vitro* Antioxidant Activity. The DPPH assay works under the mechanism of SET and HAT and is considered a mixed-mode assay.[51] The conjugates and parent compounds were observed for a duration of 120 min to demonstrate the changes in antioxidant capacity over time[52] (Figure 7A).

The data shown in Figure 7A indicated that vanillin and NM10 exhibited no antioxidant activity before 15 and 45 min, respectively. NM15 demonstrated activity only after 60 min. Once antioxidant activity was evident, the IC_{50} values exhibited a decrease over time, indicating a progressive increase in antioxidant activity. DPPH functions as both a radical initiator and an oxidizing agent. DPPH color can be lost by radical reaction (HAT) or reduction (SET) as well as unrelated events, and steric accessibility is a significant factor in determining the reaction. Hence, small compounds with greater access to the radical site have a greater antioxidant capacity.[53] This could explain why NM10 and NM15 take longer to exhibit antioxidant activity.

NM10 and NM15 exhibited strong radical scavenging activity compared to vanillin. The IC_{50} values for PDCs were significantly lower (from 435.9 to 510.4 μg/mL ($p < 0.0001$)) when compared to the starting compounds employed in the synthesis, namely vanillin (IC_{50} = 909.9 ± 93 μg/mL), which correspond to a previously published value (IC_{50} = 1397 ± 3.8 μg/mL)[54] and PAH (no activity). Furthermore, PAA, HEXNAP, N5, and N10 showed no antioxidant activity (data not shown).

Figure 7B shows a significant increase in the antioxidant activity of vanillin after conjugation to PAH. However, this increase in potency was further exemplified when considering the difference in vanillin % attachment in each compound. For example, as per elemental analysis % attachment data (Section 3.1) only 17.8% of vanillin was attached in the NM15 conjugate, thus the adjusted NM15 is more potent than vanillin ($p <$ 0.0001, Figure 7C).

The enhanced antioxidant activities of NM10 and NM15, despite their lower total phenolic content (Section 3.2), are novel finding. This suggests that the conjugation not only retains but significantly enhances the antioxidant properties of vanillin. As conjugates are Schiff bases, the presence of C = N linkage in Schiff bases is important for biological activity, including antibacterial, anticancer, and antioxidant activity.[55] Hence, the presence of an HC = N linkage within the conjugates plays a significant role in augmenting the antioxidant activity. Scipioni et al.[18] reported that the nitrogen molecule exerts the most significant influence on the radical scavenging properties, suggesting the importance of the electron pair on the nitrogen atoms for the radical scavenging property. To the best of our knowledge, no previous studies have shown that such conjugation significantly enhances the activity of vanillin. This novel finding emphasizes the significance and impact of the research, providing new insights into the potential of polymer-vanillin conjugates as potent antioxidant agents.

The FRAP assay relies on the reduction of the ferric-tripyridyltriazine $[Fe^{III}(TPTZ)_2]^{3+}$ complex. FRAP assay works on the SET mechanism.[51] The results obtained for the FRAP assay performed on the conjugates are presented in Figure 7D. All conjugates synthesized, exhibited significantly lower activity ($p < 0.0001$) when compared with vanillin (102.5 ± 11 mgTE/1 g) (Figure 7D). As stated previously, the presence of the imine moiety in the conjugates had an effect on the antioxidant activity. Even after the conjugates were adjusted as per % attachment, the conjugates did not show improved antioxidant activity compared to vanillin. This can be accounted for as it is known that Schiff bases are stable in alkaline conditions, under acidic conditions hydrolysis to the corresponding amine and carbonyl compounds[56] as has been shown in the UV study (Section 3.1). As the FRAP assay works under an acidic pH (pH 3.6), the conjugates undergo hydrolysis, and the imino bond is separated into vanillin and PAH. PAA, HEXNAP, N5, and N10 showed no FRAP activity (data not shown). However, NM15 was selected as the lead conjugate for further work, as there was no significant difference between the antioxidant activity of NM10 and NM15.

In conclusion, the enhanced antioxidant activity observed in NM10 and NM15, despite their lower total phenolic content, underscores the effectiveness of conjugating vanillin to PAH. The presence of the imino bond in Schiff bases plays a significant role in enhancing the antioxidant activity. Although the FRAP assay results indicate some limitations due to hydrolysis, the overall findings highlight the potential of PAH-vanillin

https://doi.org/10.1021/acs.chemmater.4c01767
Chem. Mater. 2024, 36, 10514−10527

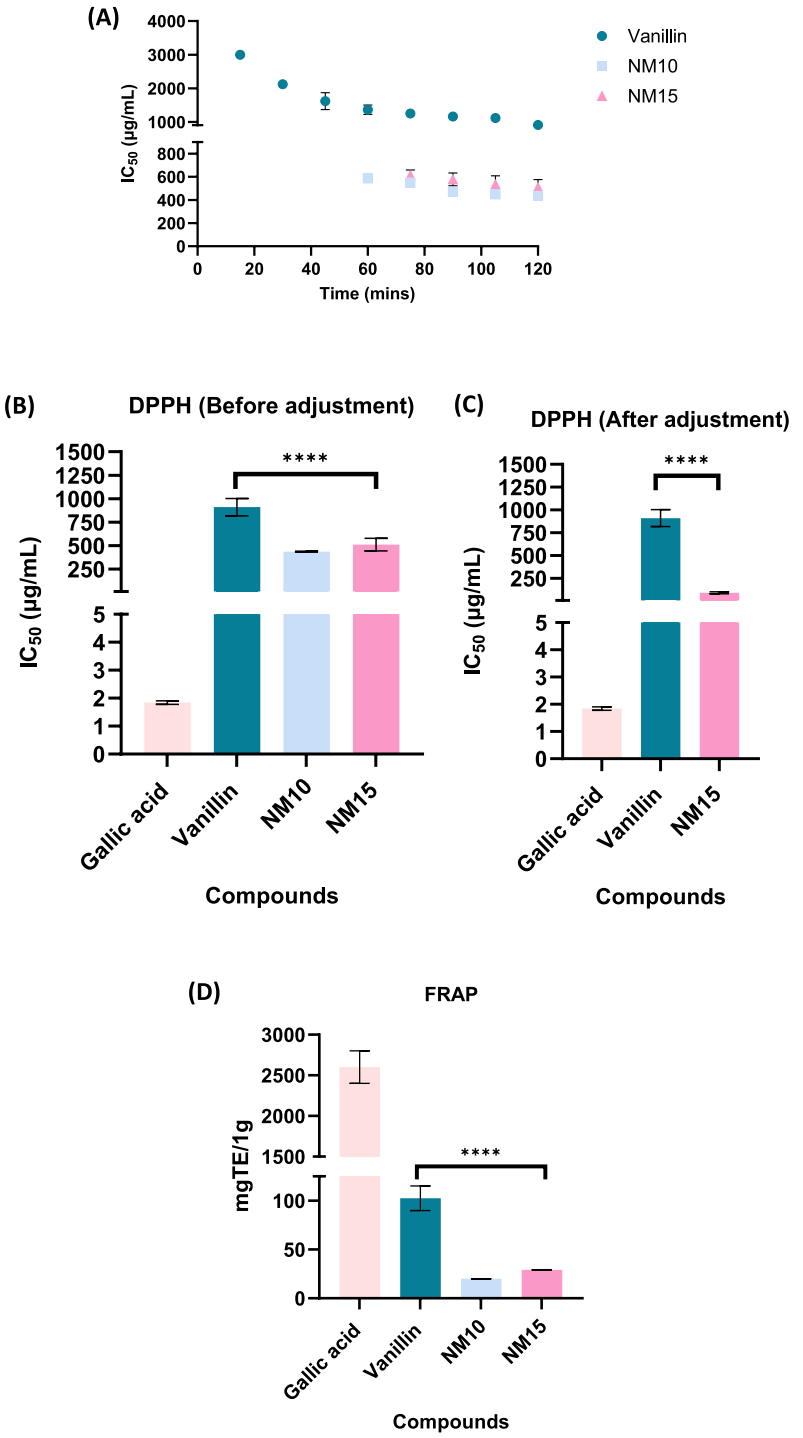

Figure 7. Antioxidant activity of vanillin, NM10, and NM15 over 120 min (A), DPPH antioxidant activity of NM10 and NM15 after 120 min before adjustment (B), after adjustment for NM15 (C), and FRAP antioxidant activity of NM10 and NM15 (D). Data presented as mean ± SD (n = 3), significant difference *via* one-way ANOVA (****$p \leq 0.0001$), and Dunnett's multiple comparisons tests.

conjugates as effective antioxidant agents. This approach provides novel insights into the development of potent antioxidant compounds.

3.4. *In Vitro* Cholinesterase Inhibitory Activity. *3.4.1. Ellman's Activity.* Ellman's Assay Involves the Hydrolysis of the Substrate AChEI/BuChEI by AChE/BuChE.

Figure 8 showed the evaluation of N5, N10, and the starting materials against the AChE and BuChE enzymes (Figure 8A,B). Both N5 and N10 showed significantly decreased activity ($p <$ 0.0001) compared to HEXNAP (Figure 8A,B). It is crucial to note, however, that HEXNAP has a relatively low solubility in water, which makes it a poor candidate for drug development;[24] thus, conjugating it to PAA not only increases its water-solubility but also produces a PDC that has anticholinesterase activity. Based on the elemental analysis % attachment data (Section 3.1), only 1.04% of HEXNAP is attached in the N5 conjugate, thus the adjusted N5 is more potent than HEXNAP ($p < 0.0001$, Figure 8C,D). However, N5 was selected as the lead conjugate

https://doi.org/10.1021/acs.chemmater.4c01767
Chem. Mater. 2024, 36, 10514−10527

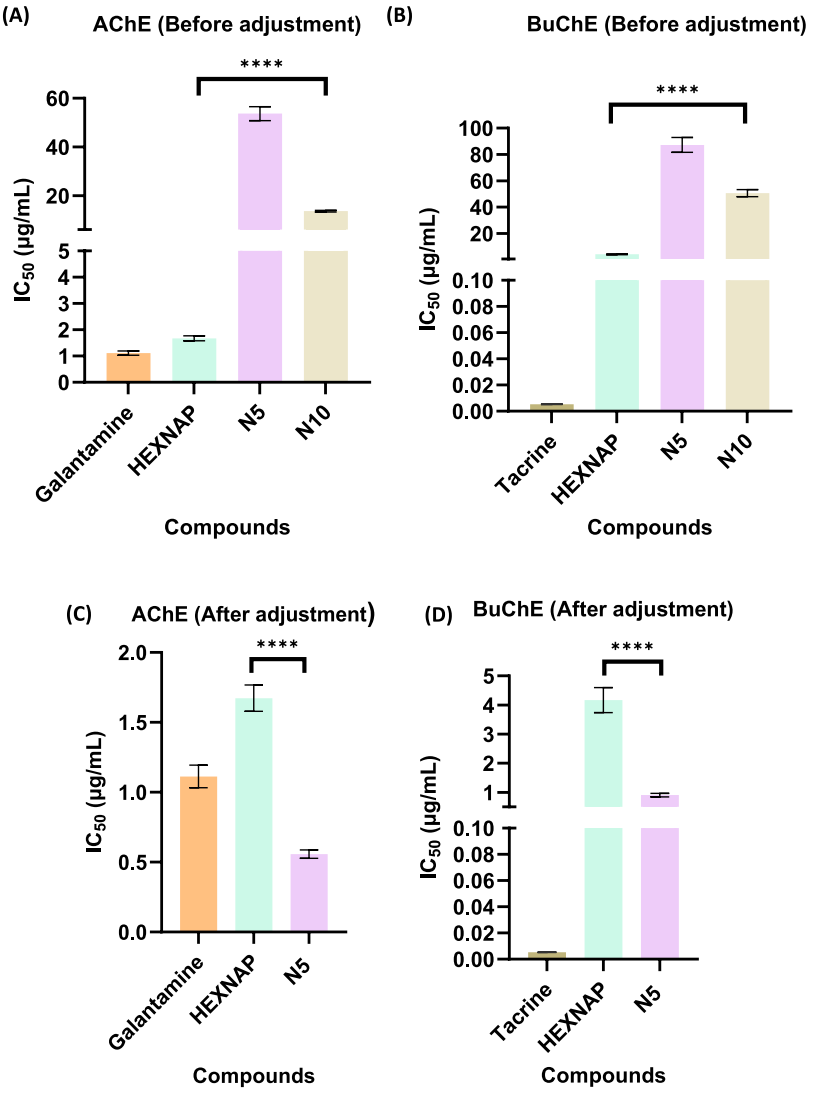

Figure 8. Ellman's AChE and BuChE inhibitory activity of N5 and N10 before adjustment (A, B) and after adjustment for N5 (C, D). Data presented as mean ± SD (n = 3), significant difference *via* one-way ANOVA (****$p \leq 0.0001$), and Dunnett's multiple comparisons tests.

for further work because only 1.04% of HEXNAP attached to PAA demonstrated significantly greater potency compared to that of HEXNAP alone. These findings are novel, as no previous studies have reported conjugates of HEXNAP with enhanced anticholinesterase activity and improved solubility.

Additionally, N5, N10, and HEXNAP showed stronger activity against AChE than BuChE. This was expected as the flexible hexyl group in HEXNAP is responsible for increased inhibitory action against AChE.[9,57] The flexibility of the long, saturated hexyl chain allows the molecule to adopt a conformation that efficiently interacts with the active site residues of AChE, but not BuChE. In BuChE, the larger and more flexible active site makes it difficult for the hexyl chain to form efficient interactions, thus, decreasing its inhibitory effectiveness.[9] This was further confirmed by *in silico* molecular modeling studies (Section 3.4.3). Furthermore, PAA, vanillin, NM15, and PAH showed no cholinesterase inhibitory activity (data not shown).

The selective inhibition of AChE over BuChE suggests that these novel PDCs can increase acetylcholine (ACh) levels in the brain, offering symptomatic relief for NDs. While initial findings suggest strong AChE inhibition, the goal of these novel conjugates is to target BuChE and reduce the risk of adverse effects associated with BuChE inhibitors.

3.4.2. Kinetic Study of BuChE Inhibition. Reversible enzymatic inhibitors may act *via* a competitive, noncompetitive, mixed, or uncompetitive mechanism.[58] Lineweaver−Burke plots can be used in the kinetic study to determine the kind of inhibition by analyzing the V_{max} and K_m values. The V_{max} is the enzyme reaction's maximal rate, whereas the K_m is the substrate concentration that equals half the V_{max}. The type of inhibitor is determined by comparing its values to those of the control (no inhibition). Competitive inhibitors are characterized by an increase in the K_m value, while the V_{max} remains unchanged. Noncompetitive inhibitors typically result in a decrease in V_{max}, with no significant change in K_m. Mixed inhibitors exhibit a decrease in the V_{max} and an increase in the K_m values. Uncompetitive inhibitors lead to a decrease in both V_{max} and K_m values as well.[58]

A kinetic study was carried out to assess the type of inhibition imparted by novel anticholinesterase conjugate N5. The BuChE enzyme was used because as AD progresses, BuChE activity increases and AChE activity declines.[12] The type of BuChE inhibition exerted by tacrine, HEXNAP, and N5 was determined

https://doi.org/10.1021/acs.chemmater.4c01767
Chem. Mater. 2024, 36, 10514−10527

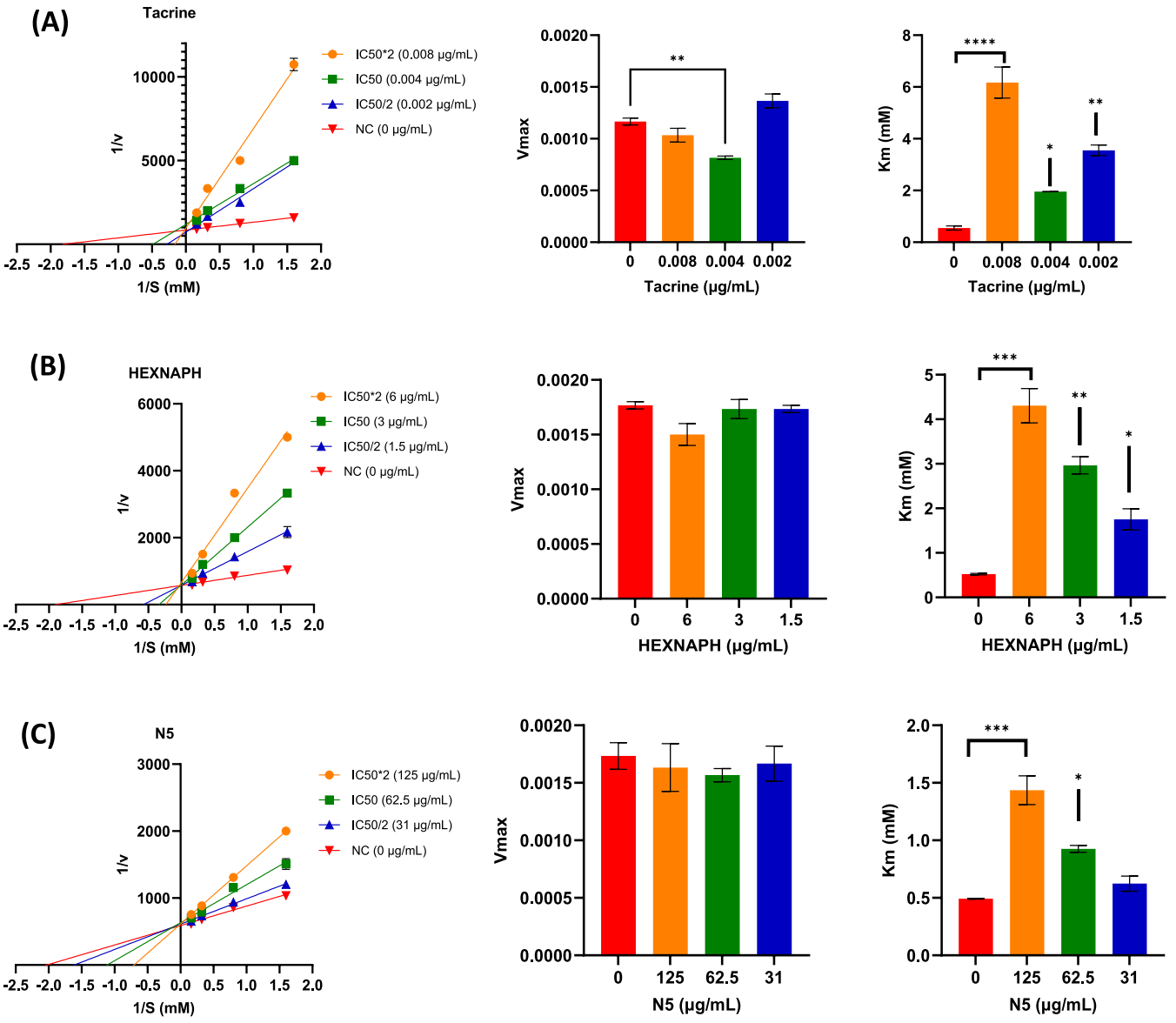

Figure 9. Ellman's BuChE kinetic study of tacrine (A), HEXNAP (B), and N5 (C). Data presented as mean ± SEM ($n = 3$), significant difference *via* one-way ANOVA (***$p \leq 0.001$ for tacrine V_{max}, HEXNAP and N5 K_m values, ****$p \leq 0.0001$ for tacrine K_m value), and Dunnett's multiple comparisons tests.

Table 4. Correlation between Binding Affinity and the *In Vitro* Results for AChE and BuChE Inhibitory Activity Using PyRx and Ellman's Assay, Respectively

	AChE		BuChE	
compounds	binding affinity (kcal/mol)	*in vitro* IC_{50} (μg/mL)	binding affinity (kcal/mol)	*in vitro* IC_{50} (μg/mL)
N5	−10	0.56 ± 0.03 (after adjustment)	−8.8	0.91 ± 0.06 (after adjustment)
HEXNAP	−9.0	1.67 ± 0.1	−9.0	4.17 ± 0.4
galantamine	−9.1	1.11 ± 0.08	NA	NA
tacrine	NA	NA	−8.8	0.0053 ± 0.0001

using Lineweaver−Burke plots. The V_{max} and K_m values were then calculated based on these plots (Figure 9).

The kinetic study revealed that both HEXNAP and N5 act as competitive inhibitors, as indicated by their V_{max} and K_m values (Figure 9B,C). The IC_{50} value of HEXNAP exhibited a V_{max} of 0.0017 and a K_m of 2.965 mM, compared to the negative control which had a V_{max} of 0.0018 and a K_m of 0.523 mM. Similarly, IC_{50} value of N5 exhibited a V_{max} of 0.0016 and a K_m of 0.926 mM, while the negative control had a V_{max} of 0.0017 and a K_m of 0.492 mM. While the V_{max} values for both HEXNAP and N5 did not differ significantly from the negative control, the K_m values were significantly higher (**$p \leq 0.01$ for HEXNAP and *$p \leq 0.05$ for N5), confirming that they competitively inhibit BuChE. Competitive inhibition is desirable in drug development for targeting BuChE because it indicates a more targeted and controlled interaction with the enzyme, which may lead to improved therapeutic effects. However, mixed inhibitors may show a more unpredictable effect as they not only compete in the

https://doi.org/10.1021/acs.chemmater.4c01767
Chem. Mater. 2024, 36, 10514−10527

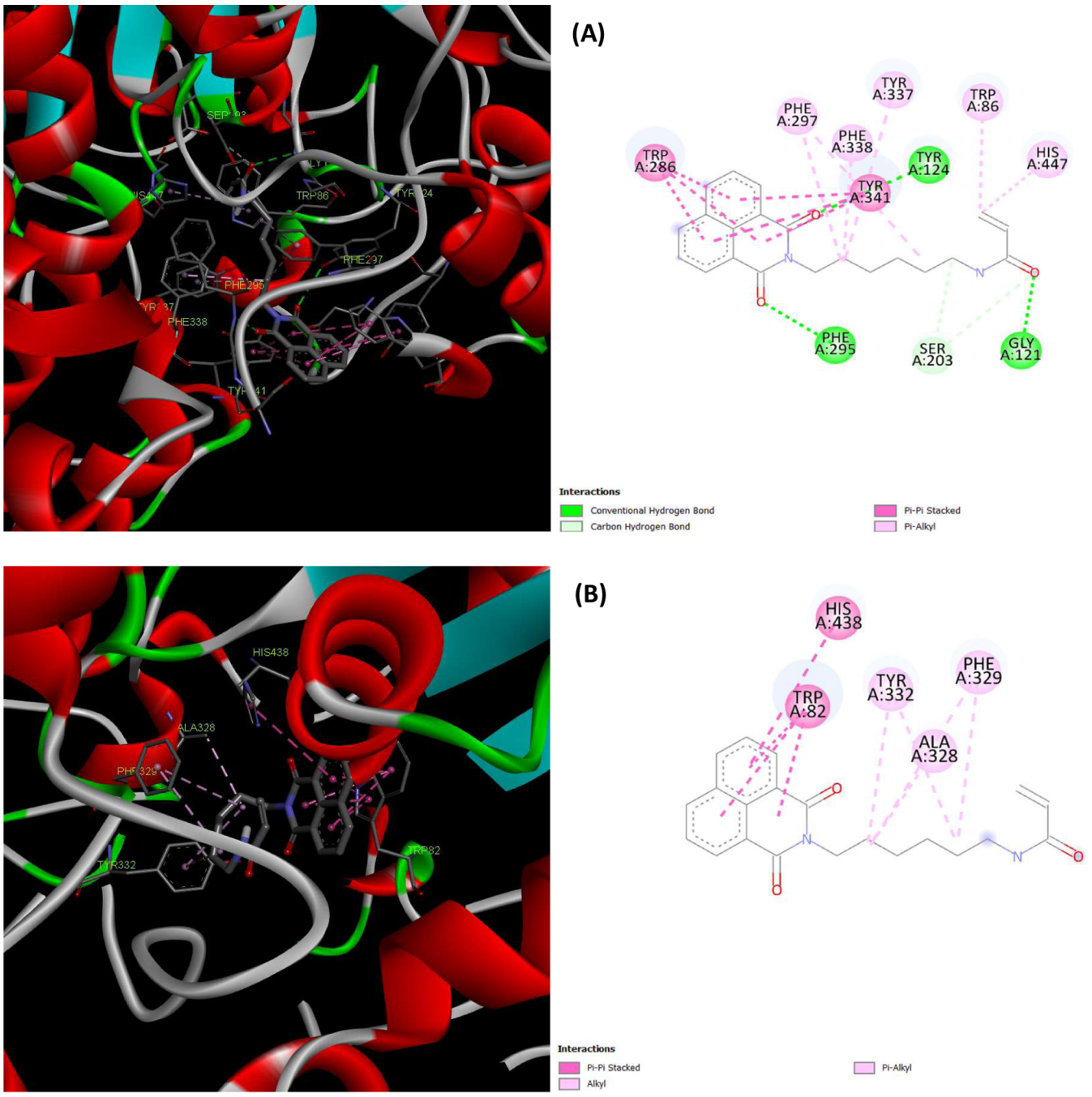

Figure 10. Binding mode of N5 in the catalytic and peripheral pocket of (A) 4PQE (hAChE) and (B) 2J4C (hBuChE).

active site but also interact with other regions of the enzyme.[58] Therefore, by competitively inhibiting BuChE, N5 could increase the levels of ACh, improving cholinergic neurotransmission and alleviating the cognitive decline linked to NDs. This finding is significant, as it represents a novel contribution to the field of PDCs for cholinesterase inhibition, with no equivalent data available in the literature.

3.4.3. Molecular Modeling. To elucidate the observed *in vitro* inhibitory effect of the compound N5 on AChE and BuChE, in comparison to HEXNAP, galantamine, and tacrine, molecular modeling studies were conducted utilizing crystal structures of ChE human isoforms. N5 exhibited a greater binding affinity for the AChE enzyme and a slightly lower affinity for the BuChE enzyme compared to HEXNAP (Table 4).

However, there may be variations between the predicted binding affinity and the *in vitro* results due to several factors. First, AChE and BuChE crystal structures from human isoforms were utilized in the docking simulations, whereas AChE and BuChE from *E. electricus* and equine serum were employed in the *in vitro* study, respectively. Second, *in silico* modeling is a simplified docking model compared to the complex human system which can result in less precise predictions of binding affinity.[59,60] Despite species differences and the ease of docking models, combining *in vitro* and *in silico* approaches is critical. *In silico* models use human enzyme structures to predict binding affinities, while *in vitro* experiments validate findings under complex conditions, improving our understanding of cholines-

https://doi.org/10.1021/acs.chemmater.4c01767
Chem. Mater. 2024, 36, 10514−10527

terase inhibitors and aiding in the development of neurological treatments.

The visualization of ligand-protein interactions between N5 and cholinesterase enzymes provided novel findings as it provided a comprehensive mechanism for how N5 inhibits hAChE and hBuChE (Figure 10).

N5, HEXNAP, and galantamine interact extensively with human AChE's (hAChE) peripheral anionic site (PAS) and catalytic anionic site (CAS), forming $\pi-\pi$ stacking bonds, hydrogen bonds, and hydrophobic interactions (Figures 10A, S19A, and S20). Notably, the polymer backbone of N5 interacts with the CAS region through π-alkyl bonds with Trp86 and His447 and forms a carbon−hydrogen bond with Ser203, contributing significantly to its inhibitory activity. This interaction indicated that the conjugation may have reoriented the molecule such that the HEXNAP portion no longer has access to the CAS site within the gorge of the hAChE compared with free HEXNAP, which interacts with the CAS site (Figure S19A). This interaction enables N5 to penetrate deeper into the enzymatic gorge, increasing its inhibitory activity compared to free HEXNAP. Overall, the longer chain (i.e., the saturated hexyl chains of HEXNAP in N5) and polymer backbone were more effective at inhibiting AChE.

Furthermore, PAS forms a stable complex with the Aβ peptide, which accelerates oligomerization and aggregation of senile plaques. Incubating AChE with Aβ peptide leads to three times more aggregation than Aβ alone.[9,61] Therefore, further work is required to determine if the binding conformation of N5 minimizes the accumulation of senile plaques.

Human BuChE (hBuChE) consists more hydrophilic and charged residues than AChE (especially in PAS sites).[61] In Figure 10B, the naphthalimide ring of N5 interacts with the CAS region *via* $\pi-\pi$ bonding with Trp82 and His438. The carbon chain of N5 interacts with CAS, forming π-alkyl bonds with Tyr332, Ala328, and Phe329. Additionally, the polymer backbone did not have any interaction with hBuChE. However, in the instance of HEXNAP (Figure S19B), identical interactions were seen with those in the N5. N5 and HEXNAP did not interact with the PAS region and did not form hydrogen bonds with hBuChE, although they did form substantial hydrophobic interactions. Tacrine produced hydrophobic and hydrogen bonds with only the CAS region (Figure S21).

Even though the active site gorge in both hAChE and hBuChE has a depth of roughly 20 Å, the volume differs by around 200 Å^3, with hBuChE being the larger isoform.[9] This could explain why the compounds interact only with CAS in hBuChE. Also, the CAS is responsible for degrading ACh.[61] Thus, conjugate N5 may be able to prevent the degradation of ACh by interacting with the CAS region of hAChE and hBuChE and can also prevent the accumulation of Aβ plaques by interacting with the PAS region in hAChE. Further work is required to confirm this in suitable *in vitro* and *in vivo* models.

This comprehensive mechanistic understanding, together with insights into the structural differences between hAChE and hBuChE, provides novel insights into the potential therapeutic benefits of novel PDC-based cholinesterase inhibitors for NDs.

4. CONCLUSIONS

This study focused on the design and synthesis of a series of novel PAH-vanillin and PAA-HEXNAP conjugates, as well as their antioxidant and cholinesterase inhibitory activity, and the exploration of their potential cholinesterase inhibitory mechanism through *in silico* molecular modeling studies. Successful conjugation of all conjugates was confirmed with ^{1}H NMR, ATR-FT-IR, and UV−visible spectroscopy. NM15 and N5 were identified as lead conjugates for further development of a polyelectrolyte complex (PEC) in the context of a multitarget strategy.[26] NM15 showed significantly enhanced *in vitro* antioxidant activity with an IC_{50} of 90.85 μg/mL (after adjustment) in the DPPH assay compared to the starting material vanillin (909.9 μg/mL), which corresponds to previously published work on vanillin.[9,18,54] Additionally, N5 showed significantly enhanced *in vitro* cholinesterase inhibitory activity with an IC_{50} of 0.56 μg/mL for AChE and 0.91 μg/mL for BuChE (after adjustment) in the Ellman's assay. Furthermore, kinetic and molecular modeling studies revealed that N5 is a competitive inhibitor of BuChE and interacts with the active sites of hAChE and hBuChE enzymes which correspond to previously published work on vanillin-naphthalimide derivatives.[9,19] However, future work is required to develop a polyelectrolyte complex (nano polyplex) by combining NM15 and N5. These NM15 and N5 complexes will be further examined for antioxidant and cholinesterase inhibitory properties, as well as *in vitro* toxicity studies. Future work will also include studies of bioavailability, pharmacokinetics, and the development of a nasal drug delivery system for the polyelectrolyte complex. This may lead to the development of novel multitarget treatment for NDs. Overall, these data suggest that PDCs are promising for developing a novel treatment for NDs.

ASSOCIATED CONTENT

Supporting Information

The Supporting Information is available free of charge at https://pubs.acs.org/doi/10.1021/acs.chemmater.4c01767.

NMR spectra; ATR-FTIR spectra; UV characterization; molecular modeling visualizations of polymer-drug conjugates and starting materials (PDF)

AUTHOR INFORMATION

Corresponding Author

Colin J. Thompson − *School of Pharmacy, Applied Sciences and Public Health, Robert Gordon University, Aberdeen AB10 7GJ, U.K.*; orcid.org/0000-0002-9571-9434; Email: c.thompson@rgu.ac.uk

Authors

Nuruddin Mahadik − *School of Pharmacy, Applied Sciences and Public Health, Robert Gordon University, Aberdeen AB10 7GJ, U.K.*

Gemma A. Barron − *School of Pharmacy, Applied Sciences and Public Health, Robert Gordon University, Aberdeen AB10 7GJ, U.K.*

Paul Kong Thoo Lin − *School of Pharmacy, Applied Sciences and Public Health, Robert Gordon University, Aberdeen AB10 7GJ, U.K.*

Complete contact information is available at: https://pubs.acs.org/10.1021/acs.chemmater.4c01767

Author Contributions

N.M.: Writing—original draft, visualization, methodology, investigation, formal analysis, data curation. G.A.B.: Supervision, writing—review and editing. P.K.T.L.: Supervision, writing—review and editing. C.J.T.: Conceptualization, supervision, funding acquisition, writing—review and editing.

Notes

The authors declare no competing financial interest.

■ ACKNOWLEDGMENTS

The authors would like to acknowledge the School of Pharmacy, Applied Sciences and Public Health at Robert Gordon University for providing their support for the completion of this work and Tenovus Scotland (G22.06 BG) for funding this work. The authors would like to further acknowledge Gray Russell (University of Aberdeen) for NMR analysis, and Eva Stueeken (Isotope Geochemistry (StAIG) laboratories, University of St Andrews) for elemental analysis.

■ REFERENCES

(1) Barnham, K. J.; Masters, C. L.; Bush, A. I. Neurodegenerative Diseases and Oxidative Stress. *Nat. Rev. Drug Discovery* **2004**, *3* (3), 205−214.

(2) Palanisamy, C. P.; Pei, J.; Alugoju, P.; Anthikapalli, N. V. A.; Jayaraman, S.; Veeraraghavan, V. P.; Gopathy, S.; Roy, J. R.; Janaki, C. S.; Thalamati, D.; Mironescu, M.; Luo, Q.; Miao, Y.; Chai, Y.; Long, Q. New Strategies of Neurodegenerative Disease Treatment with Extracellular Vesicles (EVs) Derived from Mesenchymal Stem Cells (MSCs). *Theranostics* **2023**, *13* (12), 4138−4165.

(3) Zhang, H.; Wang, Y.; Wang, Y.; Li, X.; Wang, S.; Wang, Z. Recent Advance on Carbamate-Based Cholinesterase Inhibitors as Potential Multifunctional Agents against Alzheimer's Disease. *Eur. J. Med. Chem.* **2022**, *240*, No. 114606.

(4) Van der Schyf, C. J. The Use of Multi-Target Drugs in the Treatment of Neurodegenerative Diseases. *Expert Rev. Clin. Pharmacol.* **2011**, *4* (3), 293−298.

(5) Blaikie, L.; Kay, G.; Lin, P. K. T. Current and Emerging Therapeutic Targets of Alzheimer's Disease for the Design of Multi-Target Directed Ligands. *MedChemComm* **2019**, *10* (12), 2052−2072.

(6) Walczak-Nowicka, Ł. J.; Herbet, M. Acetylcholinesterase Inhibitors in the Treatment of Neurodegenerative Diseases and the Role of Acetylcholinesterase in Their Pathogenesis. *Int. J. Mol. Sci.* **2021**, *22* (17), 9290.

(7) Bartus, R. T. On Neurodegenerative Diseases, Models, and Treatment Strategies: Lessons Learned and Lessons Forgotten a Generation Following the Cholinergic Hypothesis. *Exp. Neurol.* **2000**, *163* (2), 495−529.

(8) DeKosky, S. T. Pathology and Pathways of Alzheimer's Disease with an Update on New Developments in Treatment. *J. Am. Geriatr. Soc.* **2003**, *51* (5s2), S314−S320, DOI: 10.1046/j.1532-5415.5157.x.

(9) Blaikie, L.; Kay, G.; Lin, P. K. T. Synthesis and in Vitro Evaluation of Vanillin Derivatives as Multi-Target Therapeutics for the Treatment of Alzheimer's Disease. *Bioorg. Med. Chem. Lett.* **2020**, *30* (21), No. 127505.

(10) Tamagno, E.; Guglielmotto, M.; Vasciaveo, V.; Tabaton, M. Oxidative Stress and Beta Amyloid in Alzheimer's Disease. Which Comes First: The Chicken or the Egg? *Antioxidants* **2021**, *10* (9), 1479.

(11) Liu, Z.; Li, T.; Li, P.; Wei, N.; Zhao, Z.; Liang, H.; Ji, X.; Chen, W.; Xue, M.; Wei, J. The Ambiguous Relationship of Oxidative Stress, Tau Hyperphosphorylation, and Autophagy Dysfunction in Alzheimer's Disease. *Oxid. Med. Cell. Longevity* **2015**, *2015*, No. 352723.

(12) Mushtaq, G.; Greig, N.; Khan, J.; Kamal, M. Status of Acetylcholinesterase and Butyrylcholinesterase in Alzheimer's Disease and Type 2 Diabetes Mellitus. *CCNS Neurol. Disord.: Drug Targets* **2014**, *13* (8), 1432−1439.

(13) Chen, Z.-R.; Huang, J.-B.; Yang, S.-L.; Hong, F.-F. Role of Cholinergic Signaling in Alzheimer's Disease. *Molecules* **2022**, *27* (6), 1816.

(14) Benfeito, S.; Fernandes, C.; Vilar, S.; Remião, F.; Uriarte, E.; Borges, F. Exploring the Multi-Target Performance of Mitochondriotropic Antioxidants against the Pivotal Alzheimer's Disease Pathophysiological Hallmarks. *Molecules* **2020**, *25* (2), 276.

(15) Knez, D.; Coquelle, N.; Pišlar, A.; Žakelj, S.; Jukič, M.; Sova, M.; Mravljak, J.; Nachon, F.; Brazzolotto, X.; Kos, J.; Colletier, J.-P.; Gobec, S. Multi-Target-Directed Ligands for Treating Alzheimer's Disease: Butyrylcholinesterase Inhibitors Displaying Antioxidant and Neuroprotective Activities. *Eur. J. Med. Chem.* **2018**, *156*, 598−617.

(16) Kou, X.; Song, L.; Wang, Y.; Yu, Q.; Ju, H.; Yang, A.; Shen, R. Design, Synthesis and Anti-Alzheimer's Disease Activity Study of Xanthone Derivatives Based on Multi-Target Strategy. *Bioorg. Med. Chem. Lett.* **2020**, *30* (4), No. 126927.

(17) Makhaeva, G. F.; Kovaleva, N. V.; Rudakova, E. V.; Boltneva, N. P.; Lushchekina, S. V.; Astakhova, T. Y.; Timokhina, E. N.; Serkov, I. V.; Proshin, A. N.; Soldatova, Y. V.; Poletaeva, D. A.; Faingold, I. I.; Mumyatova, V. A.; Terentiev, A. A.; Radchenko, E. V.; Palyulin, V. A.; Bachurin, S. O.; Richardson, R. J. Combining Experimental and Computational Methods to Produce Conjugates of Anticholinesterase and Antioxidant Pharmacophores with Linker Chemistries Affecting Biological Activities Related to Treatment of Alzheimer's Disease. *Molecules* **2024**, *29* (2), 321.

(18) Scipioni, M.; Kay, G.; Megson, I.; Lin, P. K. T. Novel Vanillin Derivatives: Synthesis, Anti-Oxidant, DNA and Cellular Protection Properties. *Eur. J. Med. Chem.* **2018**, *143*, 745−754.

(19) Scipioni, M.; Kay, G.; Megson, I. L.; Lin, P. K. T. Synthesis of Novel Vanillin Derivatives: Novel Multi-Targeted Scaffold Ligands against Alzheimer's Disease. *MedChemComm* **2019**, *10* (5), 764−777.

(20) Gharai, P. K.; Khan, J.; Mallesh, R.; Garg, S.; Saha, A.; Ghosh, S.; Ghosh, S. Vanillin Benzothiazole Derivative Reduces Cellular Reactive Oxygen Species and Detects Amyloid Fibrillar Aggregates in Alzheimer's Disease Brain. *ACS Chem. Neurosci.* **2023**, *14* (4), 773−786.

(21) Sk, U. H.; Gowda, A. S. P.; Crampsie, M. A.; Yun, J. K.; Spratt, T. E.; Amin, S.; Sharma, A. K. Development of Novel Naphthalimide Derivatives and Their Evaluation as Potential Melanoma Therapeutics. *Eur. J. Med. Chem.* **2011**, *46* (8), 3331−3338.

(22) Kumar, S.; Muhammad, S.; Alarfaji, S. S.; Yoon, S.; Kim, M.; Youm, K.; Khalid, M.; Chaudhry, A. R.; Koh, J. Experimental and Computational Study of Naphthalimide Derivatives: Synthesis, Optical, Nonlinear Optical and Antiviral Properties. *Optik* **2021**, *246*, No. 167748.

(23) Zhang, Z.; Yuan, Q.; Li, M.; Bao, B.; Tang, Y. A Ratiometric Fluorescent Conjugated Oligomer for Amyloid β Recognition, Aggregation Inhibition, and Detoxification. *Small* **2021**, *17* (52), No. e2104581.

(24) Alsuraifi, A.; Lin, P.; Curtis, A.; Lamprou, D.; Hoskins, C. A Novel PAA Derivative with Enhanced Drug Efficacy in Pancreatic Cancer Cell Lines. *Pharmaceuticals* **2018**, *11* (4), 91.

(25) Dalmolin, L. F.; Khalil, N. M.; Mainardes, R. M. Delivery of Vanillin by Poly(Lactic-Acid) Nanoparticles: Development, Characterization and in Vitro Evaluation of Antioxidant Activity. *Mater. Sci. Eng., C* **2016**, *62*, 1−8.

(26) Mahadik, N.; Barron, G. A.; Lin, P. K. T.; Thompson, C. J. Polymer−Drug Conjugates as Nano-Sized Multi-Targeting Systems for the Treatment of Alzheimer's Disease. *RSC Pharm.* **2024**, *1*, 161−181.

(27) Navath, R. S.; Wang, B.; Kannan, S.; Romero, R.; Kannan, R. M. Stimuli-Responsive Star Poly(Ethylene Glycol) Drug Conjugates for Improved Intracellular Delivery of the Drug in Neuroinflammation. *J. Controlled Release* **2010**, *142* (3), 447−456.

(28) Singh, A. K.; Gothwal, A.; Rani, S.; Rana, M.; Sharma, A. K.; Yadav, A. K.; Gupta, U. Dendrimer Donepezil Conjugates for Improved Brain Delivery and Better in Vivo Pharmacokinetics. *ACS Omega* **2019**, *4* (3), 4519−4529.

(29) Duro-Castano, A.; Borrás, C.; Herranz-Pérez, V.; Blanco-Gandía, M. C.; Conejos-Sánchez, I.; Armiñán, A.; Mas-Bargues, C.; Inglés, M.; Miñarro, J.; Rodríguez-Arias, M.; García-Verdugo, J. M.; Viña, J.; Vicent, M. J. Targeting Alzheimer's Disease with Multimodal Polypeptide-Based Nanoconjugates. *Sci. Adv.* **2021**, *7* (13), No. eabf9180.

(30) Zhang, B.; Gao, Y.; Zhang, X.; Jiang, J.; Ren, J.; Wang, S.; Hu, H.; Zhao, Y.; Chen, L.; Zhao, K.; Dai, F. Ultra-Stable Dextran Conjugated Prodrug Micelles for Oxidative Stress and Glycometabolic Abnormality

Combination Treatment of Alzheimer's Disease. *Int. J. Biol. Macromol.* **2022**, *203*, 430−444.
(31) Naki, T.; Matshe, W. M. R.; Balogun, M. O.; Sinha Ray, S.; Egieyeh, S. A.; Aderibigbe, B. A. Polymer Drug Conjugates Containing Memantine, Tacrine and Cinnamic Acid: Promising Nanotherapeutics for the Treatment of Alzheimer's Disease. *J. Microencapsul.* **2023**, *40* (1), 15−28.
(32) Boussif, O.; Delair, T.; Brua, C.; Veron, L.; Pavirani, A.; Kolbe, H. V. J. Synthesis of Polyallylamine Derivatives and Their Use as Gene Transfer Vectors in Vitro. *Bioconjug. Chem.* **1999**, *10* (5), 877−883.
(33) Zhao, H. C.; Wu, X. T.; Tian, W. W.; Ren, S. T. Synthesis and Thermal Property of Poly(Allylamine Hydrochloride). *Adv. Mat Res.* **2010**, *150*−*151*, 1480−1483.
(34) Pereira, P.; Jorge, A. F.; Martins, R.; Pais, A. A. C. C.; Sousa, F.; Figueiras, A. Characterization of Polyplexes Involving Small RNA. *J. Colloid Interface Sci.* **2012**, *387* (1), 84−94.
(35) Arkaban, H.; Barani, M.; Akbarizadeh, M. R.; Pal Singh Chauhan, N.; Jadoun, S.; Dehghani Soltani, M.; Zarrintaj, P. Polyacrylic Acid Nanoplatforms: Antimicrobial, Tissue Engineering, and Cancer Theranostic Applications. *Polymers* **2022**, *14* (6), 1259.
(36) Ekladious, I.; Colson, Y. L.; Grinstaff, M. W. Polymer−Drug Conjugate Therapeutics: Advances, Insights and Prospects. *Nat. Rev. Drug Discovery* **2019**, *18* (4), 273−294.
(37) Wang, L.; Wang, X.; Xu, M.; Chen, D.; Sun, J. Layer-by-Layer Assembled Microgel Films with High Loading Capacity: Reversible Loading and Release of Dyes and Nanoparticles. *Langmuir* **2008**, *24* (5), 1902−1909.
(38) Pohl, F.; Goua, M.; Bermano, G.; Russell, W. R.; Scobbie, L.; Maciel, P.; Lin, P. K. T. Revalorisation of Rapeseed Pomace Extracts: An in Vitro Study into Its Anti-Oxidant and DNA Protective Properties. *Food Chem.* **2018**, *239*, 323−332.
(39) Huerta-Madroñal, M.; Caro-León, J.; Espinosa-Cano, E.; Aguilar, M. R.; Vázquez-Lasa, B. Chitosan − Rosmarinic Acid Conjugates with Antioxidant, Anti-Inflammatory and Photoprotective Properties. *Carbohydr. Polym.* **2021**, *273*, No. 118619.
(40) Marin, L.; Stoica, I.; Mares, M.; Dinu, V.; Simionescu, B. C.; Barboiu, M. Antifungal Vanillin−Imino-Chitosan Biodynameric Films. *J. Mater. Chem. B* **2013**, *1* (27), 3353.
(41) Balachandran, V.; Parimala, K. Vanillin and Isovanillin: Comparative Vibrational Spectroscopic Studies, Conformational Stability and NLO Properties by Density Functional Theory Calculations. *Spectrochim. Acta, Part A* **2012**, *95*, 354−368.
(42) El-Meligy, M. A.; Valachová, K.; Juránek, I.; Tamer, T. M.; Šoltés, L. Preparation and Physicochemical Characterization of Gelatin−Aldehyde Derivatives. *Molecules* **2022**, *27* (20), 7003.
(43) Waliszewski, K. N.; Pardio, V. T.; Ovando, S. L. A Simple and Rapid HPLC Technique for Vanillin Determination in Alcohol Extract. *Food Chem.* **2007**, *101* (3), 1059−1062.
(44) Zheng, S.; Liu, G. Polymeric Emissive Materials Based on Dynamic Covalent Bonds. *Molecules* **2022**, *27* (19), 6635.
(45) Liew, C.-W.; Ng, H. M.; Numan, A.; Ramesh, S. Poly(Acrylic Acid)−Based Hybrid Inorganic−Organic Electrolytes Membrane for Electrical Double Layer Capacitors Application. *Polymers* **2016**, *8* (5), 179.
(46) Singh, A.; Thotakura, N.; Singh, B.; Lohan, S.; Negi, P.; Chitkara, D.; Raza, K. Delivery of Docetaxel to Brain Employing Piperine-Tagged PLGA-Aspartic Acid Polymeric Micelles: Improved Cytotoxic and Pharmacokinetic Profiles. *AAPS PharmSciTech* **2019**, *20* (6), 220.
(47) Kollár, J.; Hrdlovič, P.; Chmela, Š.; Sarakha, M.; Guyot, G. Synthesis and Transient Absorption Spectra of Derivatives of 1,8-Naphthalic Anhydrides and Naphthalimides Containing 2,2,6,6-Tetramethylpiperidine; Triplet Route of Deactivation. *J. Photochem. Photobiol., A* **2005**, *170* (2), 151−159.
(48) Fante, C.; Greco, F. Polymer-Drug Conjugates. In *Fundamentals of Pharmaceutical Nanoscience*; Uchegbu, I. F.; Schätzlein, A. G.; Cheng, W. P.; Lalatsa, A., Eds.; Springer: New York, NY, 2013; pp 159−182.
(49) Aryal, S.; Baniya, M. K.; Danekhu, K.; Kunwar, P.; Gurung, R.; Koirala, N. Total Phenolic Content, Flavonoid Content and Antioxidant Potential of Wild Vegetables from Western Nepal. *Plants* **2019**, *8* (4), 96.
(50) Anouar, E. A Quantum Chemical and Statistical Study of Phenolic Schiff Bases with Antioxidant Activity against DPPH Free Radical. *Antioxidants* **2014**, *3* (2), 309−322.
(51) Munteanu, I. G.; Apetrei, C. Analytical Methods Used in Determining Antioxidant Activity: A Review. *Int. J. Mol. Sci.* **2021**, *22* (7), 3380.
(52) Tai, A.; Sawano, T.; Yazama, F.; Ito, H. Evaluation of Antioxidant Activity of Vanillin by Using Multiple Antioxidant Assays. *Biochim. Biophys. Acta Gen Subj.* **2011**, *1810* (2), 170−177.
(53) Prior, R. L.; Wu, X.; Schaich, K. Standardized Methods for the Determination of Antioxidant Capacity and Phenolics in Foods and Dietary Supplements. *J. Agric. Food Chem.* **2005**, *53* (10), 4290−4302.
(54) Fayeulle, A.; Trudel, E.; Damiens, A.; Josse, A.; Youssef, N. B. H.; Vigneron, P.; Vayssade, M.; Rossi, C.; Ceballos, C. Antimicrobial and Antioxidant Activities of Amines Derived from Vanillin as Potential Preservatives: Impact of the Substituent Chain Length and Polarity. *Sustainable Chem. Pharm.* **2021**, *22*, No. 100471.
(55) Kumar, M.; Padmini, T.; Ponnuvel, K. Synthesis, Characterization and Antioxidant Activities of Schiff Bases Are of Cholesterol. *J. Saudi Chem. Soc.* **2017**, *21*, S322−S328.
(56) Cordes, E. H.; Jencks, W. P. The Mechanism of Hydrolysis of Schiff Bases Derived from Aliphatic Amines. *J. Am. Chem. Soc.* **1963**, *85* (18), 2843−2848.
(57) Gao, J.; Midde, N.; Zhu, J.; Terry, A. V.; McInnes, C.; Chapman, J. M. Synthesis and Biological Evaluation of Ranitidine Analogs as Multiple-Target-Directed Cognitive Enhancers for the Treatment of Alzheimer's Disease. *Bioorg. Med. Chem. Lett.* **2016**, *26* (22), 5573−5579.
(58) Palmer, T.; Bonner, P. L. Enzyme Inhibition. In *Enzymes*; Elsevier, 2011; pp 126−152.
(59) Kasteel, E. E. J.; Nijmeijer, S. M.; Darney, K.; Lautz, L. S.; Dorne, J. L. C. M.; Kramer, N. I.; Westerink, R. H. S. Acetylcholinesterase Inhibition in Electric Eel and Human Donor Blood: An in Vitro Approach to Investigate Interspecies Differences and Human Variability in Toxicodynamics. *Arch. Toxicol.* **2020**, *94* (12), 4055−4065.
(60) Pantsar, T.; Poso, A. Binding Affinity via Docking: Fact and Fiction. *Molecules* **2018**, *23* (8), 1899.
(61) Pourshojaei, Y.; Abiri, A.; Eskandari, K.; Haghighijoo, Z.; Edraki, N.; Asadipour, A. Phenoxyethyl Piperidine/Morpholine Derivatives as PAS and CAS Inhibitors of Cholinesterases: Insights for Future Drug Design. *Sci. Rep.* **2019**, *9* (1), No. 19855.

https://doi.org/10.1021/acs.chemmater.4c01767
Chem. Mater. 2024, 36, 10514−10527

Supporting Information

Synthesis and Evaluation of Polymer-Drug Conjugates as Potential Antioxidants and Cholinesterase Inhibitors for Neurodegenerative Diseases

Nuruddin Mahadik, Gemma A. Barron, Paul Kong Thoo Lin, Colin J. Thompson*

School of Pharmacy, Applied Sciences and Public Health, Robert Gordon University, Aberdeen, UK, AB10 7GJ

*Corresponding author

Colin J. Thompson (c.thompson@rgu.ac.uk)

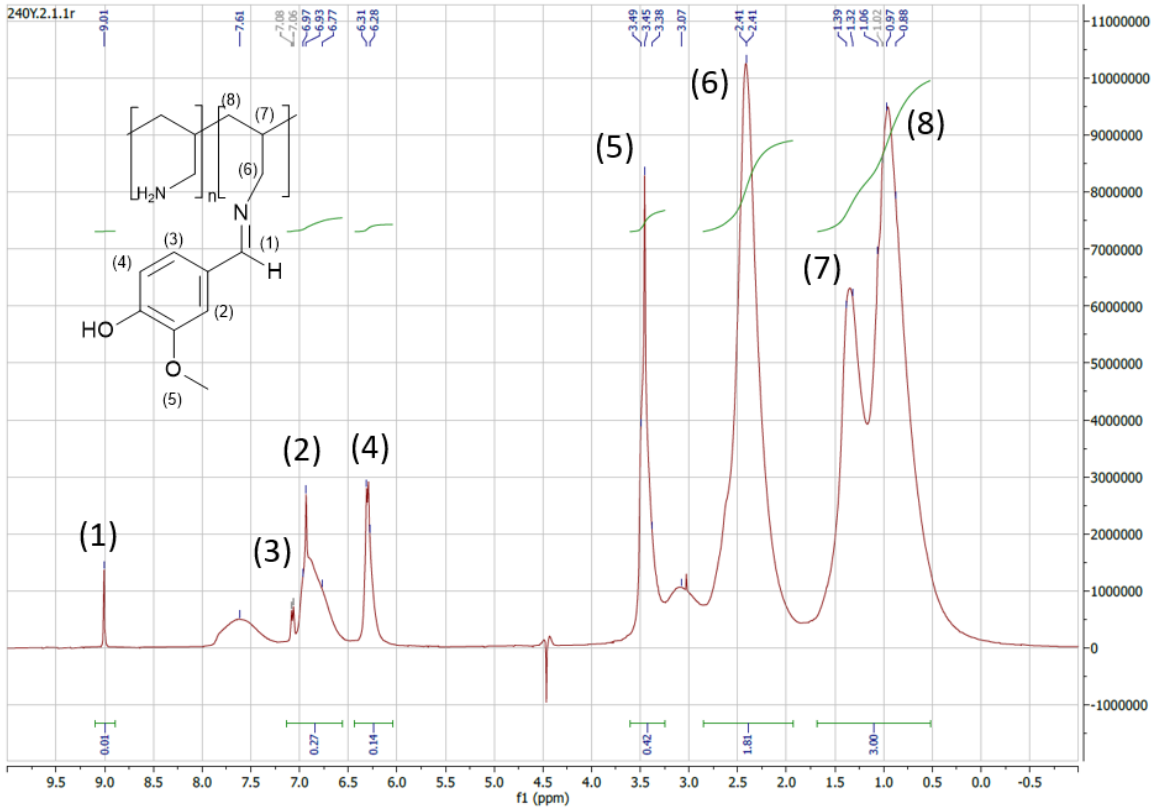

Figure S1. ^{1}H NMR spectra of NM15.

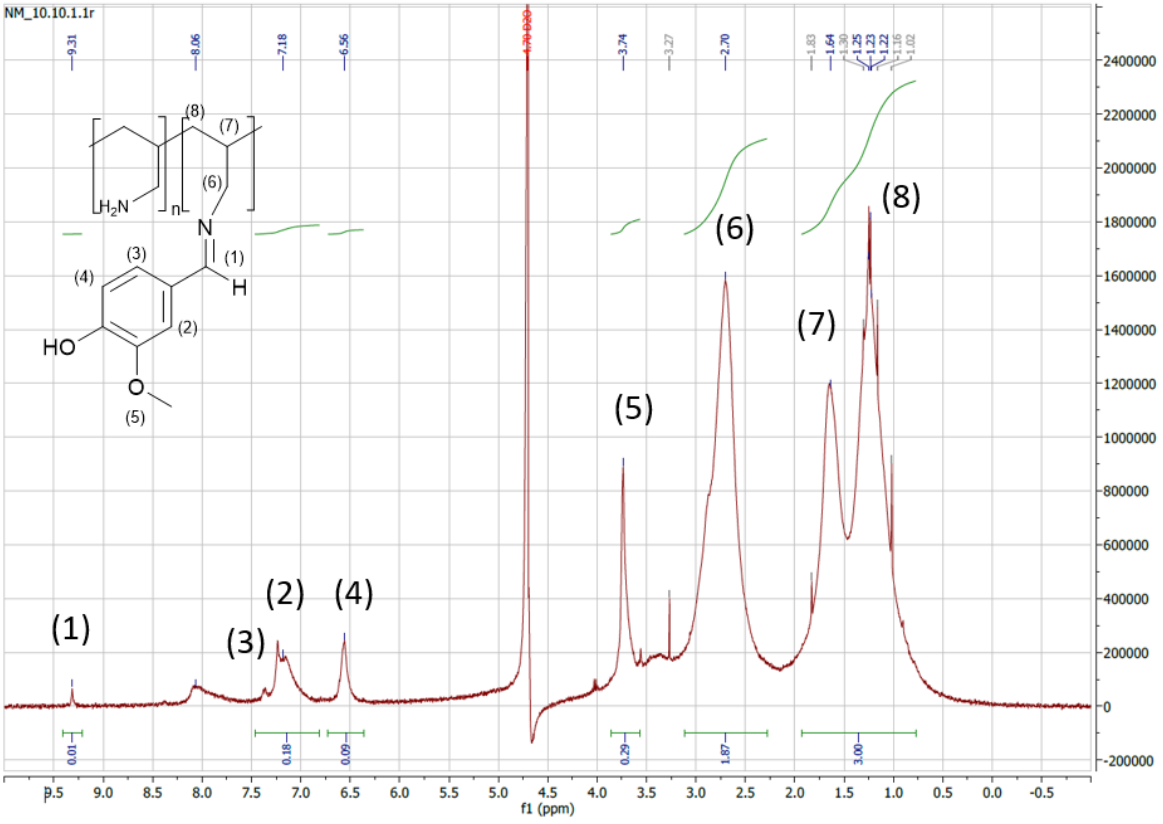

Figure S2. ^{1}H NMR spectra of NM10.

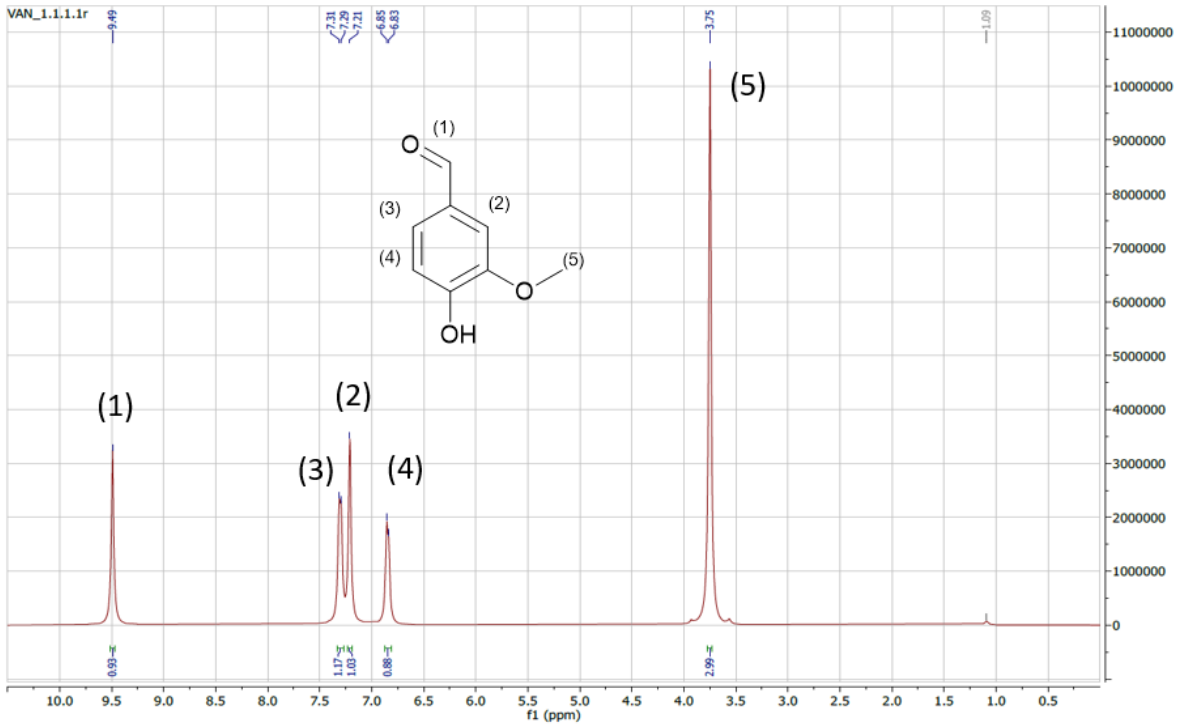

Figure S3. ^{1}H NMR spectra of Vanillin**.**

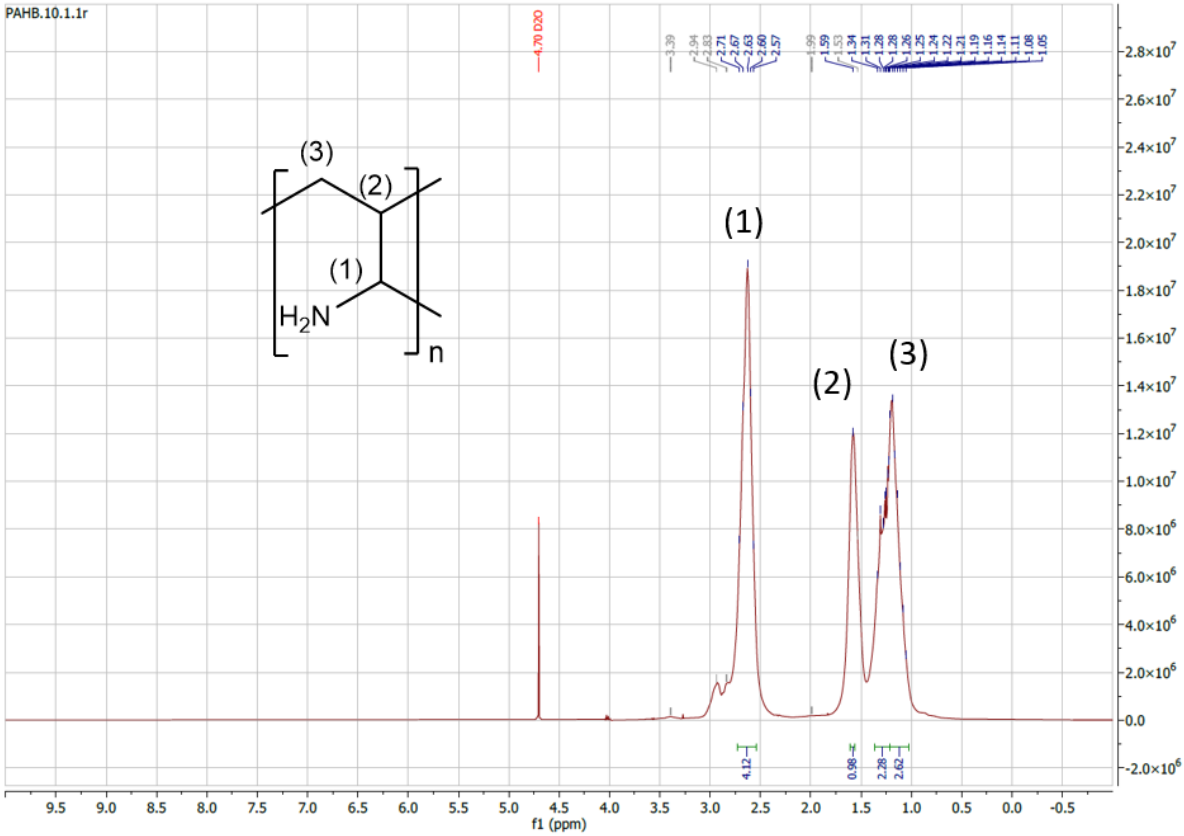

Figure S4. ^{1}H NMR spectra of PAH.

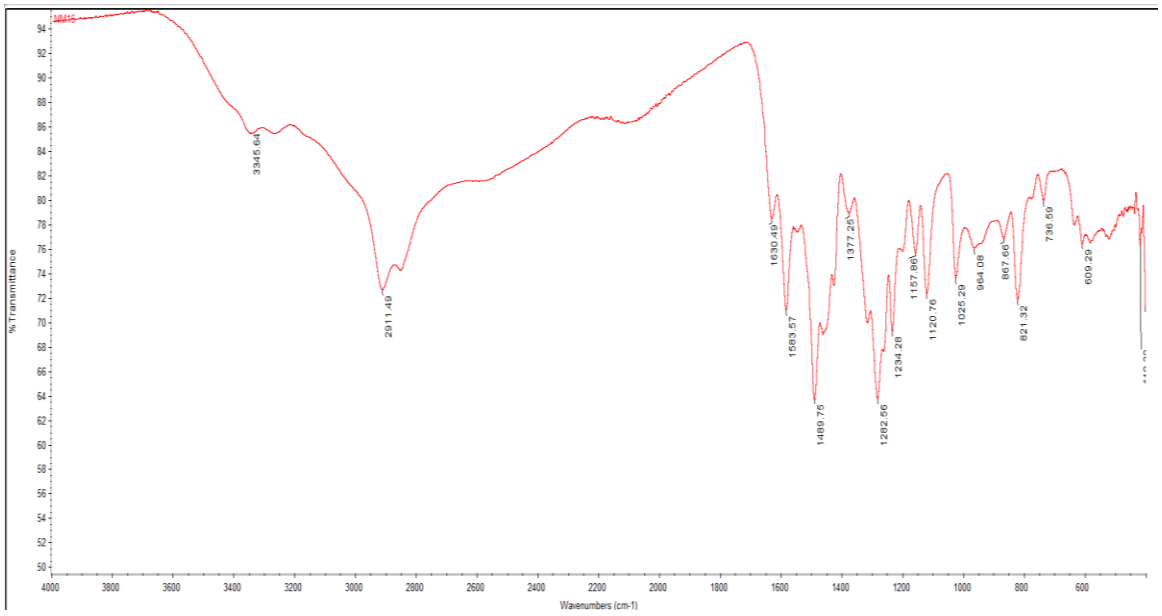

Figure S5. FTIR spectra of NM15.

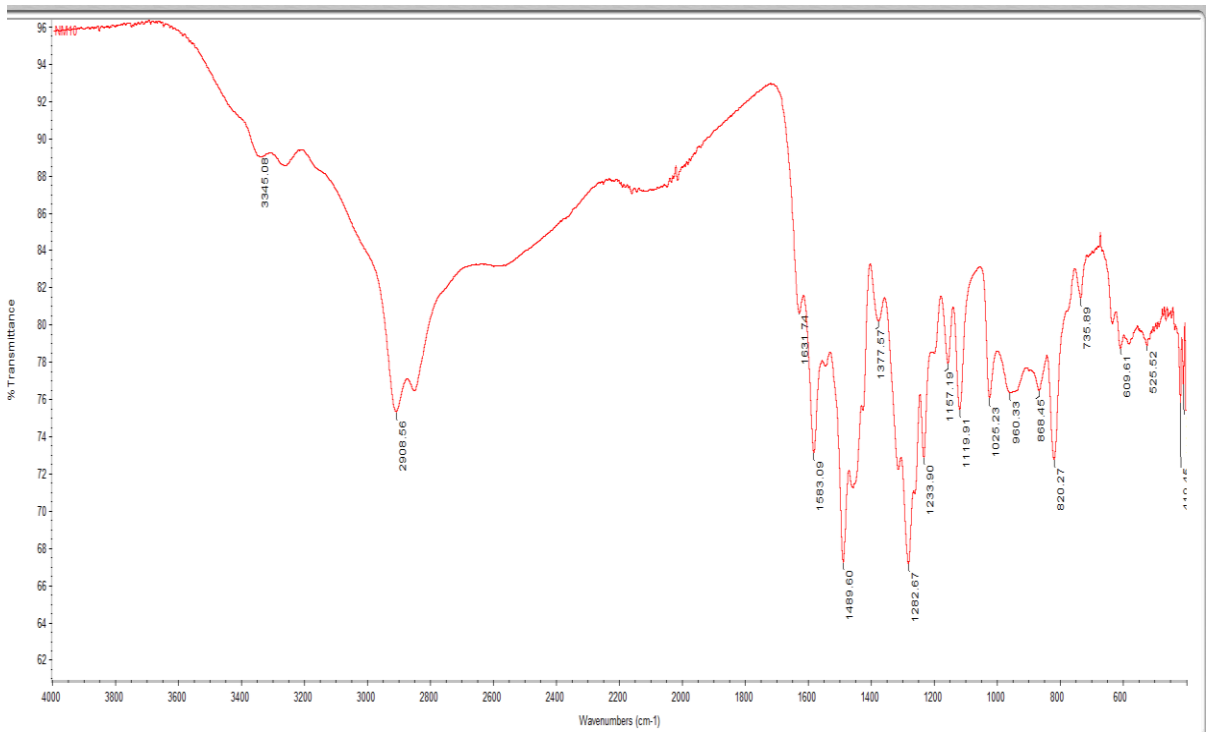

Figure S6. FTIR spectra of NM10.

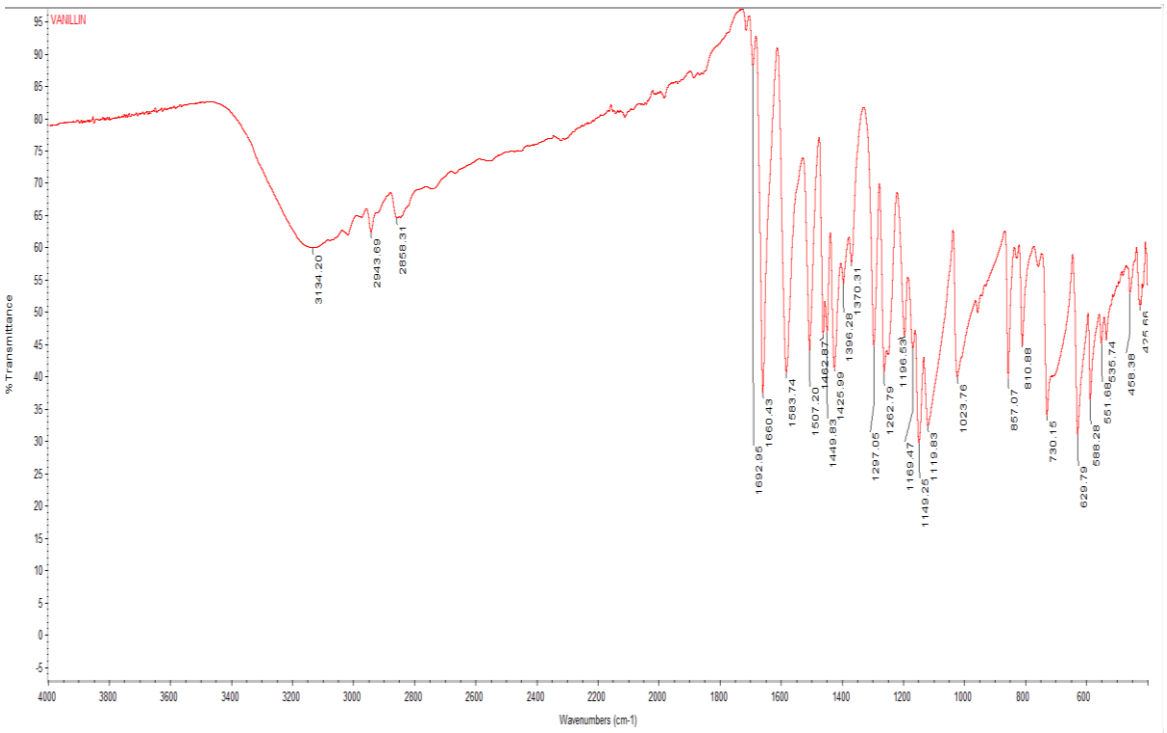

Figure S7. FTIR spectra of Vanillin.

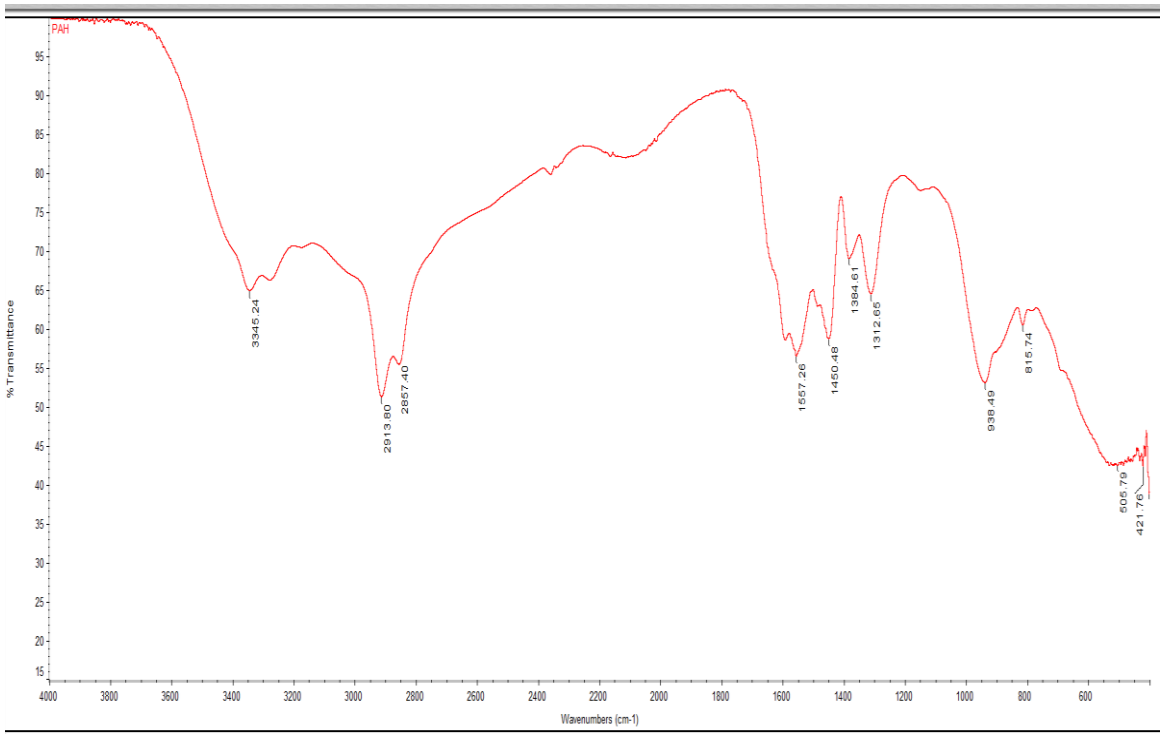

Figure S8. FTIR spectra of PAH.

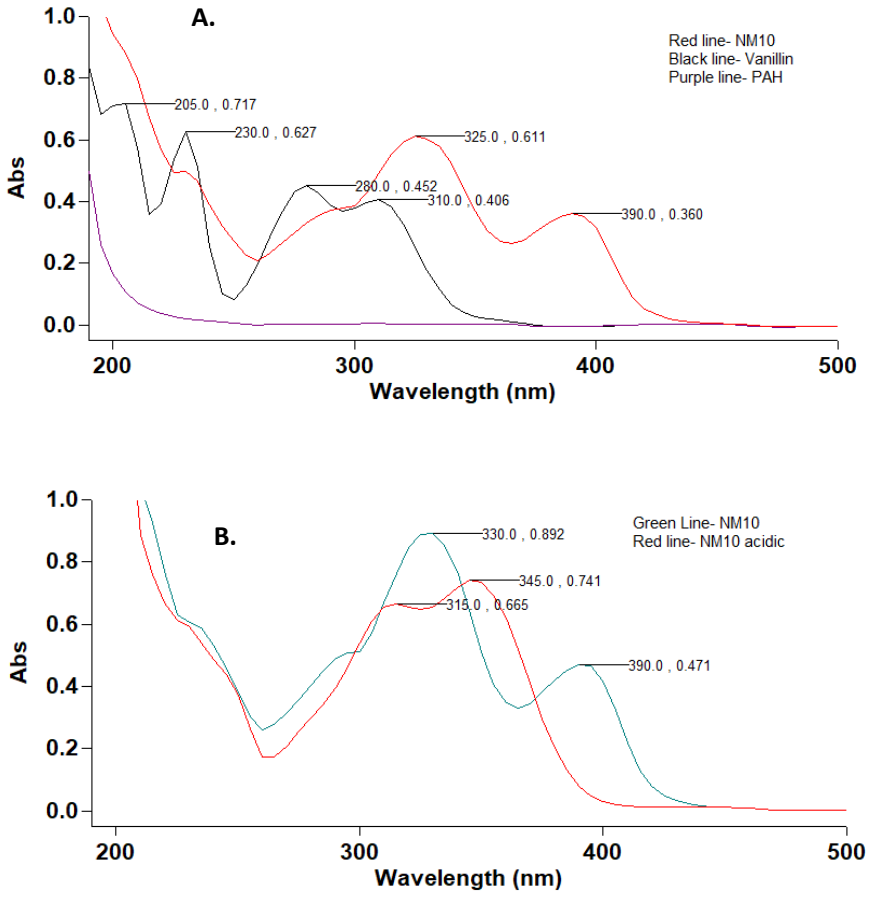

Figure S9. UV-Visible spectroscopic analysis of **A.** NM10, **B.** NM10 at acidic pH.

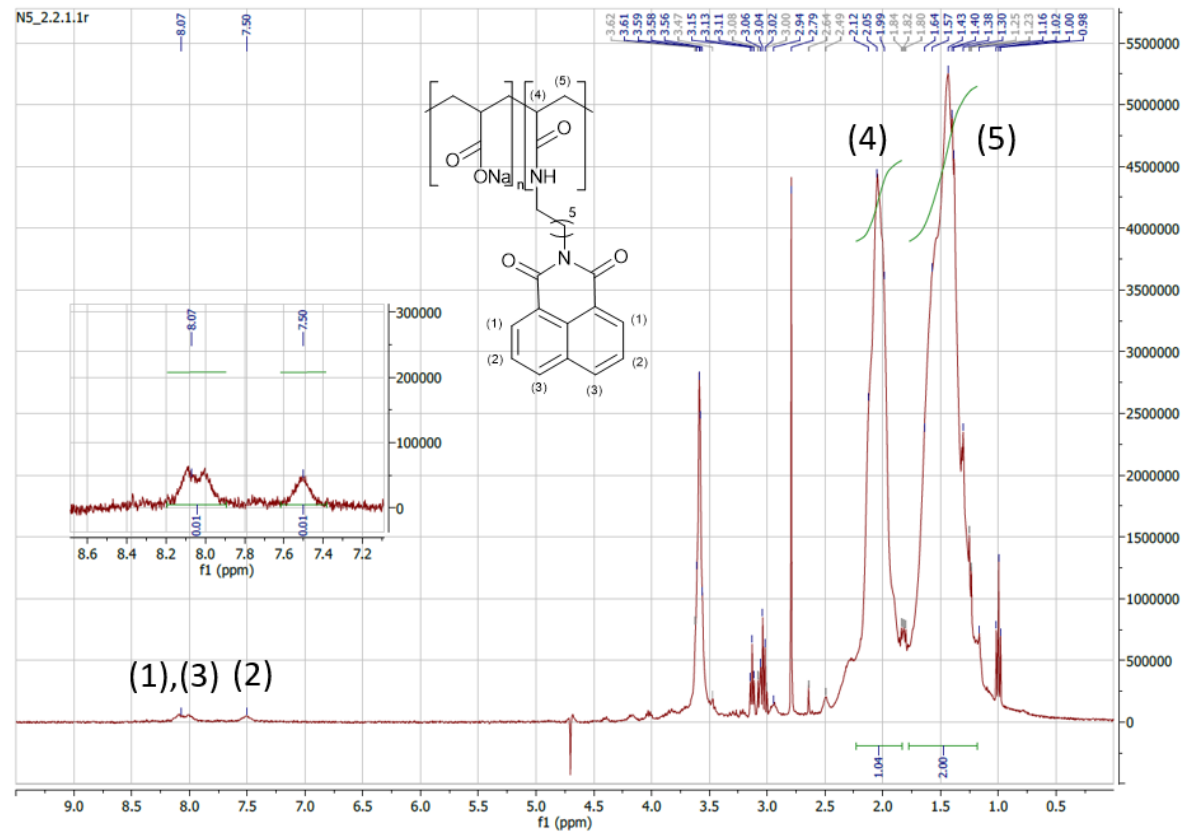

Figure S10. ^{1}H NMR spectra of N5.

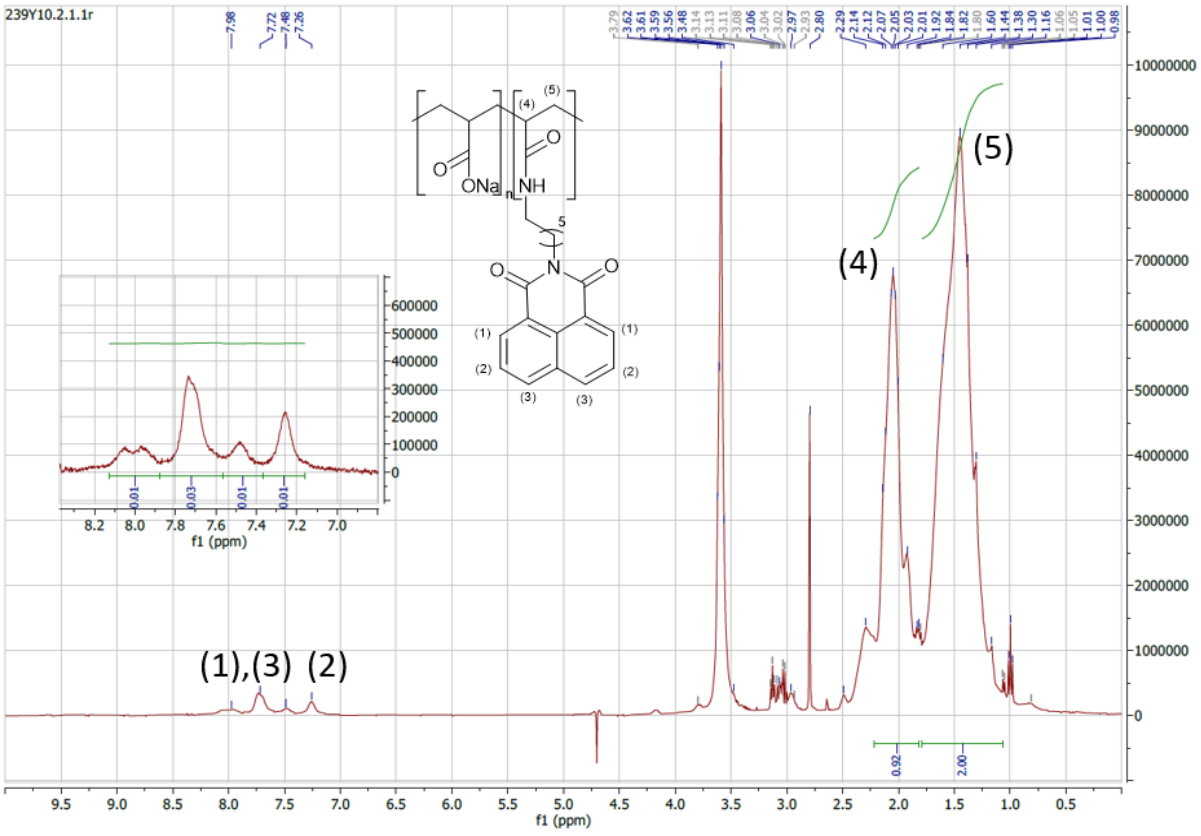

Figure S11. ^{1}H NMR spectra of N10.

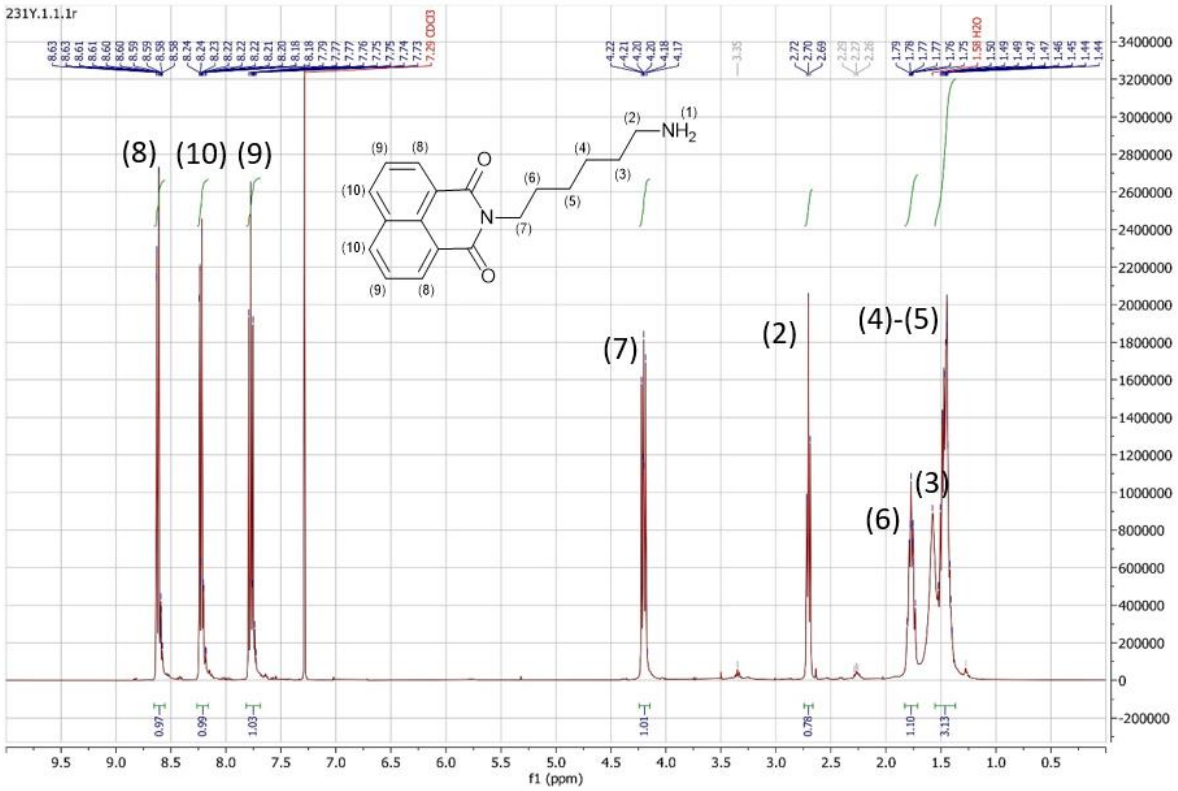

Figure S12. ^{1}H NMR spectra of HEXNAP

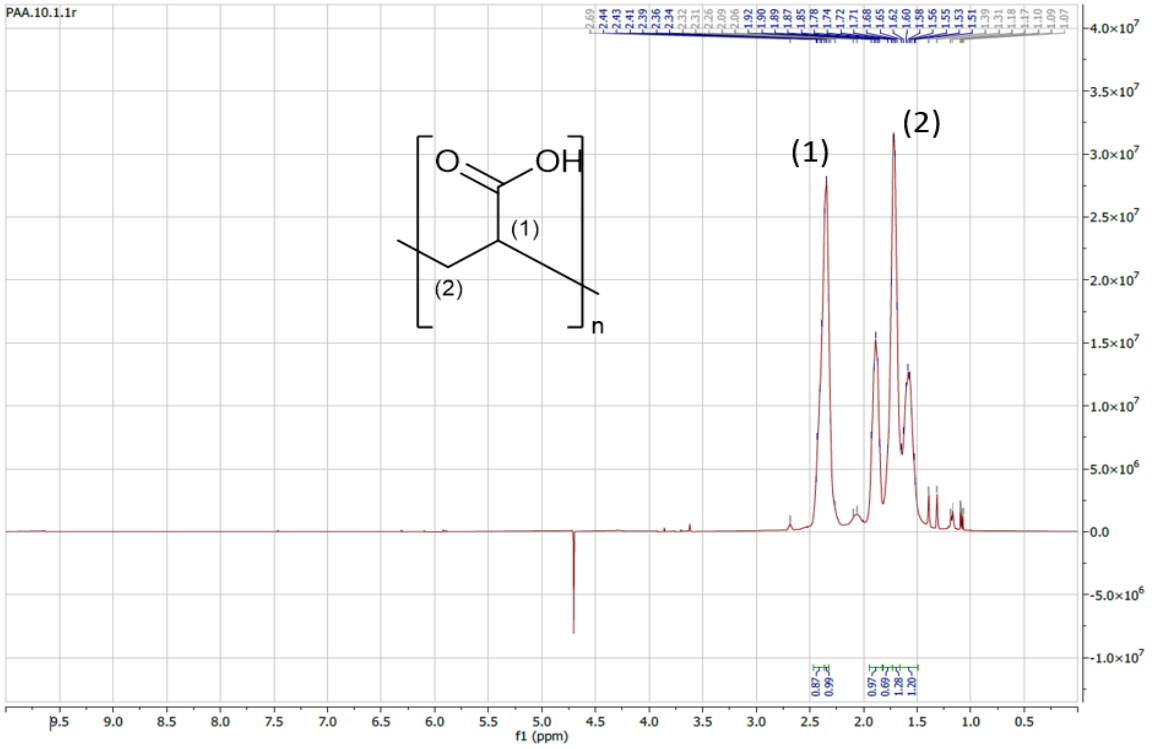

Figure S13. ^{1}H NMR spectra of PAA

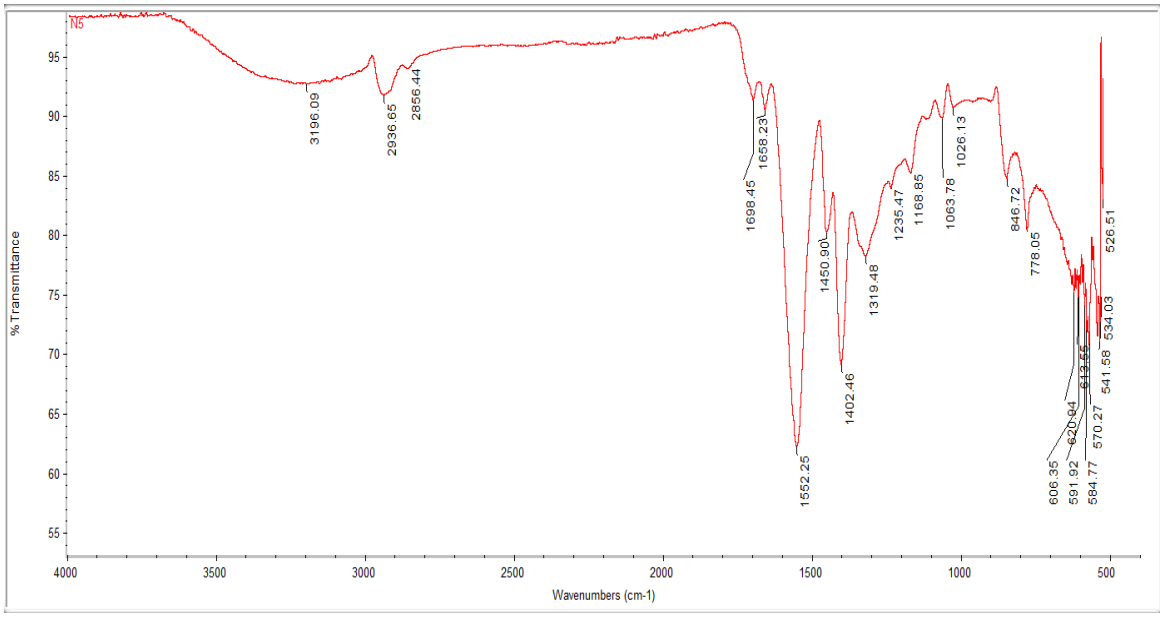

Figure S14. FTIR spectra of N5.

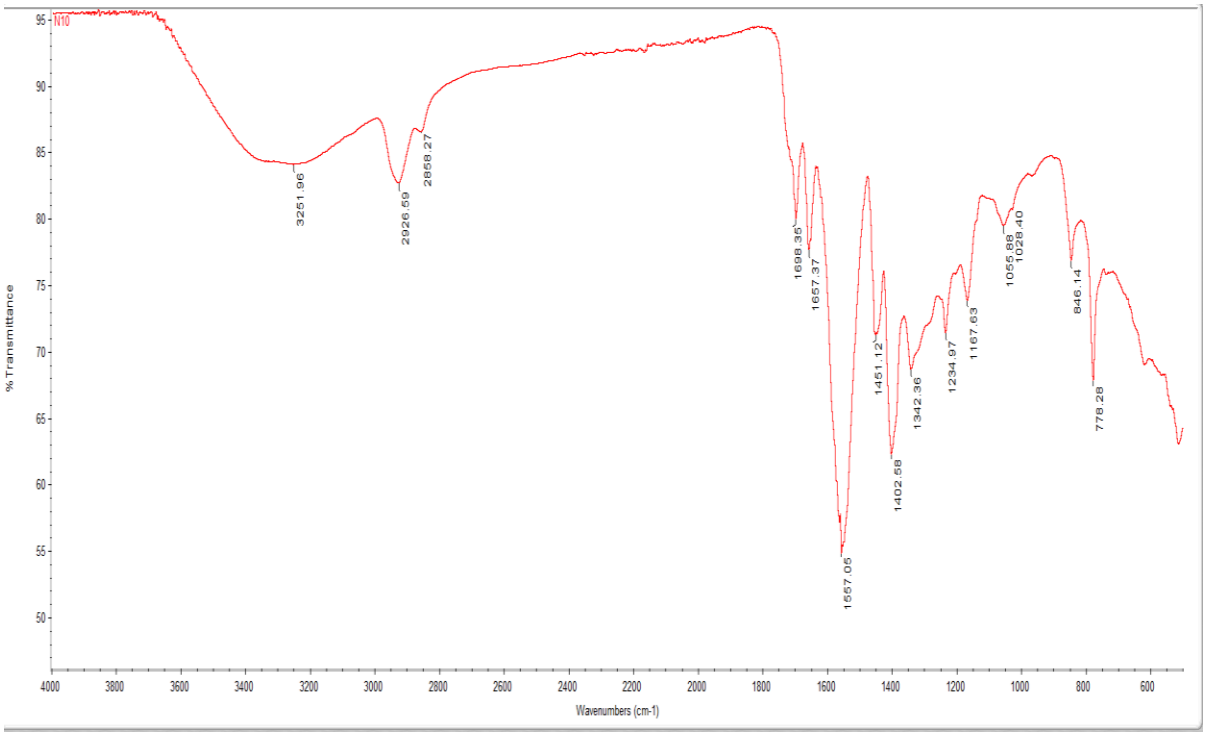

Figure S15. FTIR spectra of N10.

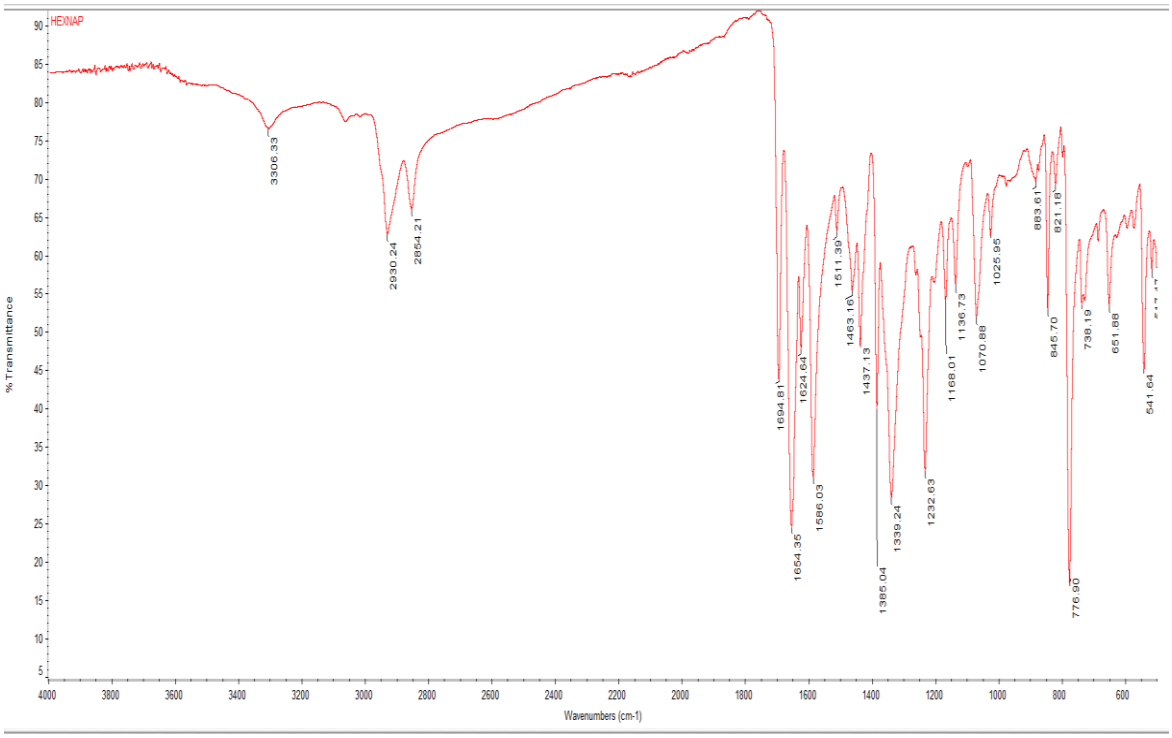

Figure S16. FTIR spectra of HEXNAP.

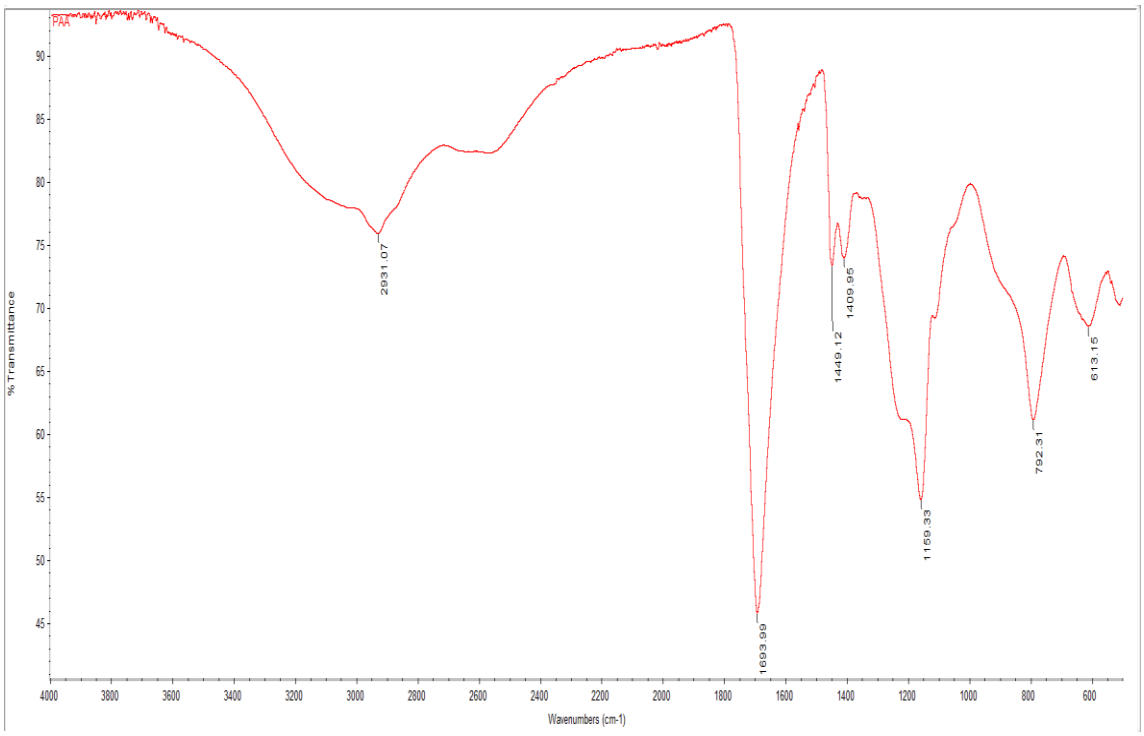

Figure S17. FTIR spectra of PAA.

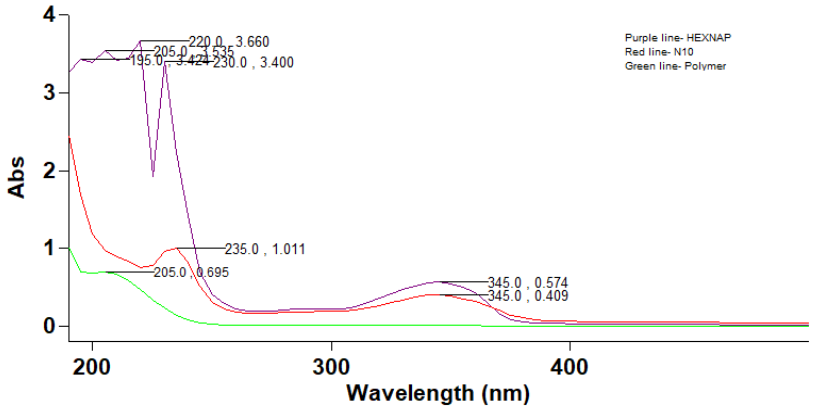

Figure S18. UV-Visible spectroscopic analysis of N10.

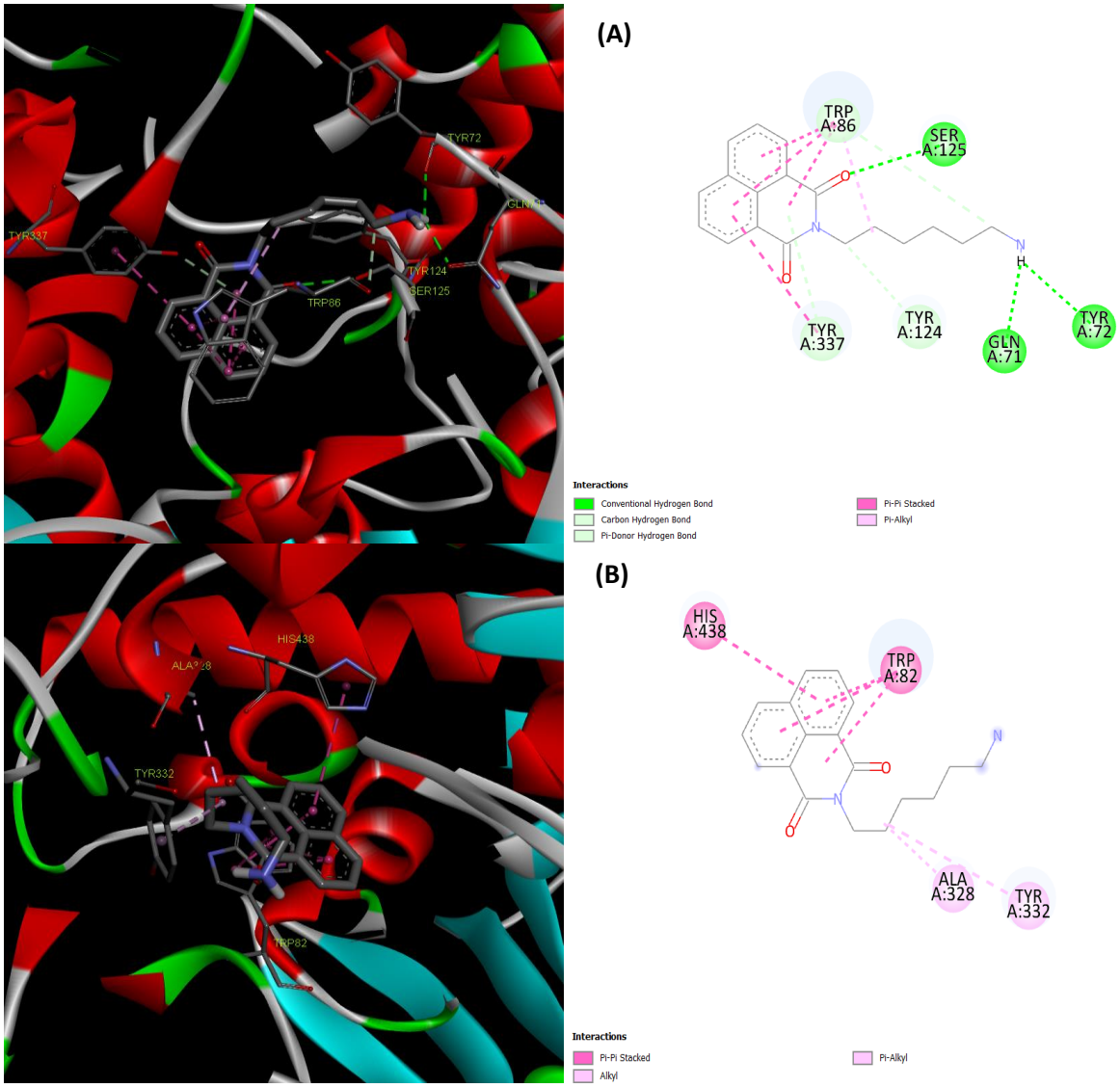

Figure S19. Binding mode of HEXNAP in the catalytic and peripheral pocket of **(A)** 4PQE (hAChE) and **(B)** 2J4C (hBuChE).

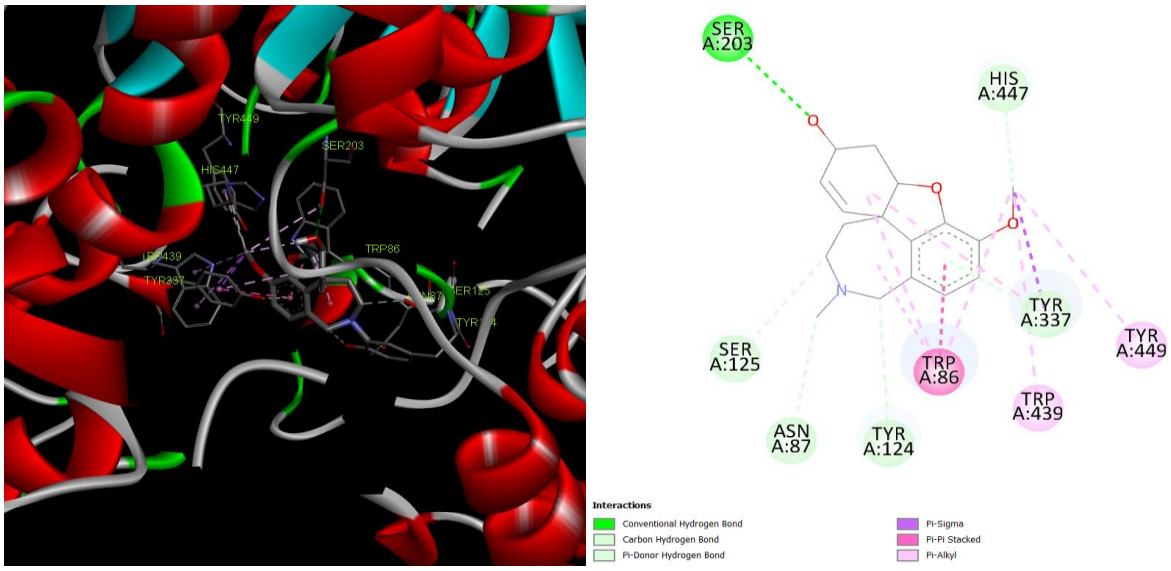

Figure S20. Binding mode of galantamine in the catalytic and peripheral pocket of 4PQE (hAChE)

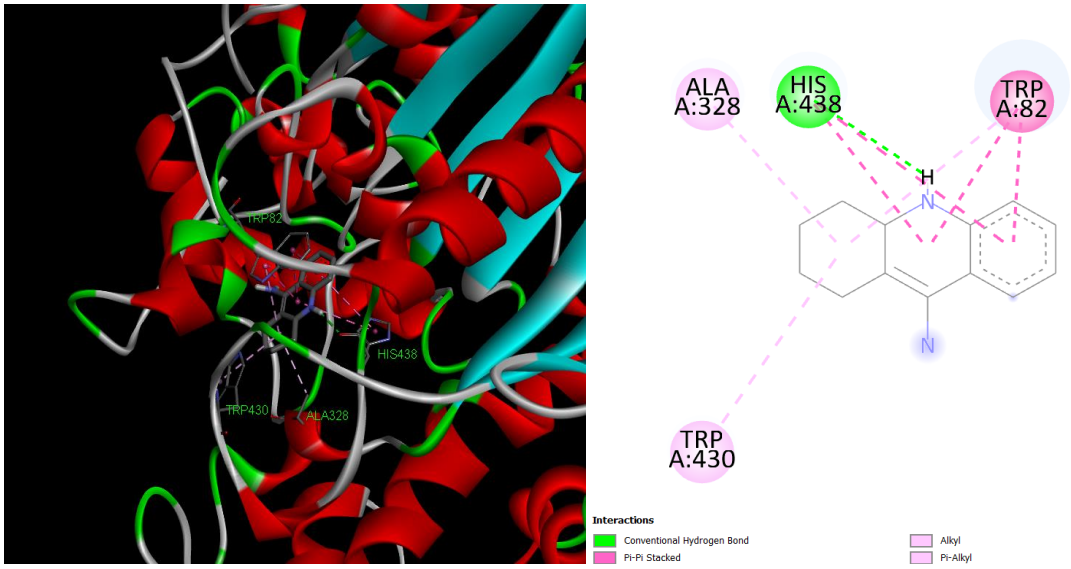

Figure S21. Binding mode of tacrine in the catalytic and peripheral pocket of 2J4C (hBuChE).